Three-Dimensional Parametric Analysis of a Switchable Vortex Generator for Aerodynamic Load Alleviation at Transonic Speeds

Marino, Luca; Eberle, Adrian ; Sodja, J.

DOI
10.2514/6.2025-0035

Publication date
2025

Document Version
Final published version

Published in
Proceedings of the AIAA SCITECH 2025 Forum

AIAA SciTech Forum
6-10 January 2025, Orlando, FL
AIAA SCITECH 2025 Forum

10.2514/6.2025-0035

Three-dimensional parametric analysis of a switchable vortex generator for aerodynamic load alleviation at transonic speeds

Luca Marino* and Jurij Sodja†
Delft University of Technology, The Netherlands

Adrian Eberle‡
Airbus Operations GmbH, Germany

This study investigates the aerodynamic performance of switchable vortex generators (SVGs) operated in spoiler configuration for load alleviation at transonic speeds. Using three-dimensional computational fluid dynamics (CFD) simulations, the effects of design parameters — including the height, aspect ratio, and spacing between the vortex vanes — are analysed on a simplified wing geometry, modelled as a straight extrusion of a supercritical airfoil. The analysis demonstrates that finite-span spoiler devices such as SVGs can effectively reduce the generated lift in cruise conditions, but their performance is strongly affected by geometric properties. Distinct aerodynamic regimes can be determined by placing a SVG of varying height and aspect ratio on the wing upper surface, characterised by different degrees of flow separation downstream of the device. Lift reduction becomes significant only when the size of the vortex vane is such to trigger full flow separation. The aerodynamic behaviour induced by a single SVG is further examined under high-speed off-design conditions, showing that larger vortex vanes induce full flow separation at lower angles of attack, while smaller SVGs can lead to sharp lift variations at higher incidence. The interaction between multiple SVGs is found to be significantly influenced by their spacing and aspect ratio, with the wall ratio emerging as a critical parameter. Smaller SVGs are most effective at high wall ratios, where they can generate a more uniform flow separation across the upper surface. In contrast, larger devices perform better at low wall ratios, where they can trigger full flow separation independently of their mutual interaction.

Nomenclature

c	=	chord-length
C_D	=	drag coefficient of the wing
C_{fx}	=	skin friction coefficient
C_l	=	sectional lift coefficient
C_L	=	lift coefficient of the wing
C_p	=	pressure coefficient
h	=	height of the vortex generator vane
M	=	Mach number
N	=	Number of employed vortex generators
Re	=	Reynolds number
w	=	width of the vortex generator vane
x	=	coordinate along the chord-wise direction
y	=	coordinate along the span-wise direction
y^+	=	dimensionless wall distance parameter
z	=	coordinate vertical direction

*Research Associate, Faculty of Aerospace Engineering, Department of Aerospace Structures and Materials, Kluyverweg 1, 2629 HS Delft; l.marino-1@tudelft.nl.

†Assistant Professor, Faculty of Aerospace Engineering, Department of Aerospace Structures and Materials, Kluyverweg 1, 2629 HS Delft; j.sodja@tudelft.nl.

‡R&T project leader, Flight Physics, Technology Strategy & Integration, Airbus-Allee 1, 28199 Bremen; adrian.eberle@airbus.com

α	=	angle of attack
Δ	=	distance between subsequent vortex generators' rotation axes
ϕ	=	wall ratio parameter

I. Introduction

The ever-growing need for a reduction of the environmental footprint of civil aviation is driving the development of disruptive new technologies for the next aircraft generation. A major contribution to this goal is expected from the employment of high-aspect-ratio (HAR) wings (AR>14), which offer significant benefits in terms of improved aerodynamic efficiency and reduced drag generation [1]. However, the use of HAR wings in modern aircraft is still limited by several challenges, including those related to their weight and flexibility. Increasing the wingspan can result in higher structural weight due to the need for additional supports and reinforcements, while reducing structural weight can increase the wing's sensitivity to gusts and manoeuvrers, due to its larger flexibility [2]. The development of novel load control technologies to be integrated within wing design represents an appealing solution for minimising the impact of gusts and manoeuvrers loads on the aircraft's structure, reducing weight requirements, and improving structural reliability.

Switchable vortex generators (SVGs) are one of the key concepts currently under development within the Clean Aviation UP Wing project to enable high performance of the outer sections of HAR wings. These devices are designed to improve aerodynamic flow control under different flight conditions. SVGs offer a dual functionality: they can alleviate aerodynamic loading on the outer wing sections in high-speed conditions, and delay flow separation in high-lift settings. As shown in Fig.1, the spoiler function of the SVG is activated by positioning the vortex vane perpendicularly to the airflow, aiming to trigger flow separation and, by this, offloading wing sections experiencing high structural stresses in high-speed conditions and/or during gusts and manoeuvrers. Conversely, rotating the vane at an angle between 0 and 90 degrees enables the vortex generator functionality, where the SVG re-energises the boundary layer and promotes downstream flow attachment through the generation of stream-wise vortices. Furthermore, the SVG can be deactivated by aligning the vortex vane parallel to the airflow, thereby minimising its aerodynamic impact.

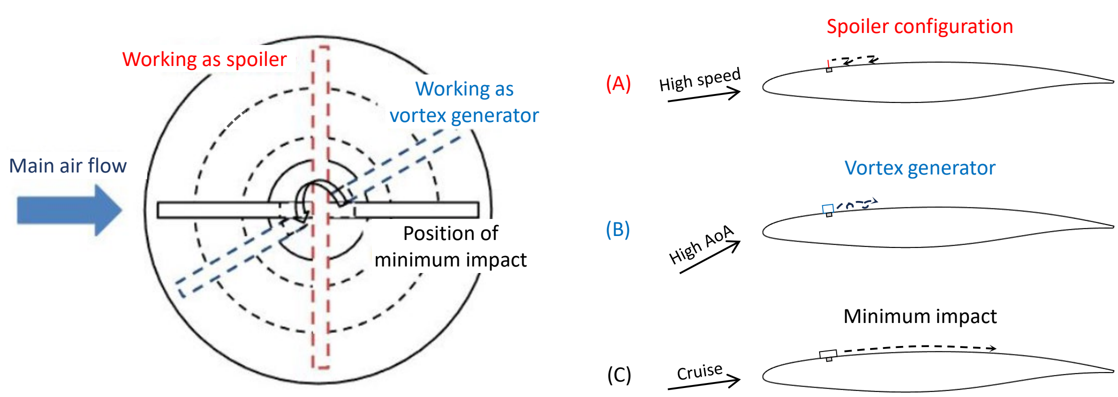

Fig. 1 Concept design of a switchable vortex generator [3].

The working principles of conventional, passive vortex generators are generally well understood. Since their first introduction in the late 1940s [4], these devices have been used to control flow separation by increasing the near-wall momentum through the transfer from the free-stream flow to the boundary layer region [5]. Extensive theoretical [6–9] and experimental [10–17] research has been conducted over the years to investigate the performance of vortex generators for varying design parameters, including their height, length, orientation and position. On the other hand, the use of devices such as spoilers or tabs for load alleviation purposes has only been explored recently, and most results have been obtained within restrictive assumptions, limiting to 2D analysis and subsonic conditions.

The concept of the mini-tab can be seen as a generalisation of the Gurney flap, which is a thin tab perpendicular to the airflow, located at the trailing edge to provide a lift increase [18]. Parametric investigations carried out for mini-tabs located on the lower surface of a NACA 0012 airfoil [19, 20] for varying height, mounting angle and chord-wise locations near trailing edge revealed that, while effective in producing a lift increase, mini-tabs of height exceeding 2% chord-length would also generate an excessive drag increase; moreover, a sweet spot for aerodynamic performance was observed for mounting angles of about 45 degrees with respect to the airfoil surface. Good performance in lift increase were also observed by applying this generalised Gurney flap to a supercritical airfoil in transonic conditions [21]. Further studies [22–25] were conducted to explore the use of active mini-tabs (1-2% chord-length) for load control in gas-turbine blades. Numerical simulations and wind-tunnel tests were performed by positioning the mini-tabs on the upper and lower surfaces of thick airfoils, in proximity of the trailing edge, observing a rapid and significant change in the generated lift when these devices were deployed in static conditions, or in response to simulated wind gusts. Baker et al. [26] investigated the effect of mini-tabs mounted on the upper surface of the airfoil for locations after 40% chord-length, observing a maximum effect in lift mitigation for locations about 60% chord-length at small incidence, and a stronger lift reduction at higher angles of attack for more forward locations of the device. Similar behaviours had already been observed by Jacobs [27], whose investigation extended to also include near-leading edge mini-tab locations, highlighting their strong effect on the $C_l - \alpha$ curve, particularly in terms of maximum lift reductions at high incidence. Heathcote et al. [28, 29] further investigated numerically and experimentally the load alleviation performance of mini-tabs placed on the upper surface of a NACA 0012 airfoil in subsonic conditions, for varying tab heights and chord-wise locations. Their studies showed that mini-tabs close to the trailing edge can provide a significant lift reduction at small incidence, but become ineffective at higher angles of incidence, while the opposite behaviour is exhibited by tabs located near the leading edge. Locations around 60% chord-length proved effective for a larger range of angles of attack, while stronger effects were generally detected for higher mini-tabs. Bull [30] and Hadjipantelis [31] studied experimentally the load alleviation performance provided by mini-spoiler placed on the upper surface near the leading edge to understand the effects of unsteady wing plunging motion, showing that these devices remain highly effective if the plunge velocity and the amplitude of the unsteady effect are not too large. In particular, Hadjipantelis et al. [31] focused on the effect of three-dimensionality by accounting for single and multiple finite-span mini-spoilers placed on a finite wing at various span-wise locations. The results showed that the load alleviation performance can decay if the amplitude and/or the frequency of the oscillation increases, also showing an affinity between the behaviour of finite-spoilers and the two-dimensional mechanisms investigated in [30]. In a recent work [3], the authors of this paper carried out a 2D parametric analysis to explore the load alleviation performances of a mini-tab located on the upper surface of a supercritical airfoil in transonic conditions. While the overall effects of the mini-tab height and chord-wise position agreed well with those determined by Heathcote et al. [28, 29], additional phenomena were also observed due to transonic effects. Large mini-tabs (height above 3% chord-length) were found to perform poorly at negative incidence, generating strong normal shocks on the airfoil lower surface, while small SVGs (height below 1% chord-length) showed limited performance in cruise conditions and at high incidence, due to the generation of shock waves on the upper surface and the absence of significant induced flow separation. Although not yielding the largest lift reduction in nominal cruise conditions, mini-tabs positioned more closely to the leading edge provided a more robust lift reduction in a large range of incidence angles, while near-trailing edge locations led to sharp lift variations and early stall at higher angles of attack. Overall, the results available in the literature consistently prove the effectiveness of the use of mini-tabs and similar devices for load alleviation purposes, but also emphasise the need for a careful parameter selection during the design stage. However, further studies are still required to investigate the load alleviation performance provided by finite-span mini-tabs when operated in transonic conditions. In fact, little is known regarding the effect of parameters such as the aspect ratio, the interaction between multiple mini-tabs and, in general, specific three-dimensional flow effects which might arise around the mini-tabs in transonic conditions.

This contribution explores the aerodynamic load alleviation performance of the spoiler function of the SVG at transonic speeds, by means of three-dimensional computational fluid dynamics (CFD) simulations. The scope of this investigation is to understand how the three-dimensional flow affects the behaviour exhibited by mechanical devices such as mini-spoilers in these conditions when they only occupy a fraction of the overall wingspan. To this end, a simplified geometry is obtained by extruding a typical supercritical airfoil into a straight wing and placing one or multiple SVGs over the upper surface. The aerodynamic effects generated by a single SVG are explored for varying height and aspect ratio of the vortex vane in nominal cruise conditions and in high-speed off-design conditions characterised by different values of the angle of attack. The interaction among multiple SVGs is studied by analysing how parameters such as their number, spacing, and span-wise fraction occupied.

The remaining of this paper is organised as follows. The analysis methodology is described in Sect.II. The aerodynamic performance of a single SVG in transonic cruise conditions is investigated Sect.III, while the effect of variations of the angle of attack is analysed in Sect.IV. The interaction between two or multiple SVGs is investigated in

Sect.V, while concluding remarks are provided in Sect.VI.

II. Analysis methodology

This paper aims at investigating the effect of the vortex vane sizing parameters on the load alleviation performance provided by switchable vortex generators when operated in their spoiler configuration in high-speed conditions. In particular, since the effect of the vane height and the chord-wise position have been investigated in the authors' previous work [3], this contribution focuses on the analysis of the three-dimensional effects introduced by the presence of one or more finite-span spoiler devices on the upper surface of a high-aspect-ratio wing.

A. Geometry selection and flow conditions

This study is conducted by performing three-dimensional computational fluid dynamics (CFD) simulations in the nominal cruise conditions defined for the DLR-F25 wing, reported in Table 1, on a simplified wing geometry obtained as a straight extrusion of the wing section investigated in [3]. This wing section, consisting in a typical supercritical airfoil, is a cross-section of the DLR-F25 wing, taken at 85% wingspan and transformed according to the rule of cosine [32, 33], with steps described in detail in [3], to account for the wing sweep effects (see Fig.2). This transformation can only provide approximate results for tapered wings [34]; therefore, the aerodynamic behaviour observed in this paper is not meant to be representative of the actual performance of the DLR-F25 wing. Considering the flow conditions reported in Table 1, as well as applying the rule of cosine, the Mach and Reynolds numbers of the simulations were set to $M_\infty = 0.7064$ and $Re_\infty = 6.665 \cdot 10^{-6}$ respectively.

Table 1 Airflow properties in nominal cruise conditions for DLR-F25 wing and simplified wing geometry.

Density, kg/m^3	Temperature, K	Velocity (DLR-F25), m/s	Velocity (extruded wing), m/s	Viscosity, kg/(ms)
0.3955	220.80	232.26 ($M_\infty = 0.78$)	210.33 ($M_\infty = 0.7064$)	1.4443$\cdot 10^{-5}$

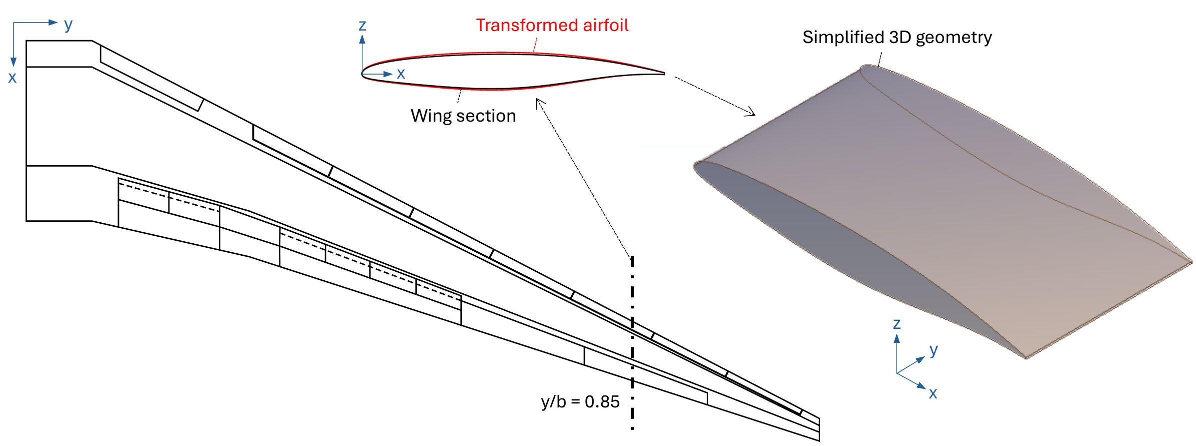

Fig. 2 Layout of the DLR-F25 wing, cross-section at 85% wingspan and simplified 3D geometry extruded along the y-axis.

B. Mesh and simulation settings

The simplified geometry of the wing, the vortex generators, and the computational domain were modelled in Ansys Design Modeler®. The dimensions of the fluid computational domain, whose geometry is shown in Fig.3, in the x- and z- directions were set to 100 times the wing section's chord-length to minimise the impact of the far-field boundary conditions on the solution. The extension of the domain along the y-direction was set equal to that of the wing extrusion, and symmetry boundary conditions were imposed on its side faces. Finally, the vortex vanes were modelled as zero-thickness thin surfaces perpendicular to the wing upper surface and aligned with the 25% chord line, and no-slip wall boundary conditions were applied. The height, width, position, and number of SVGs, as well as extruded wingspan, were adjusted based on the specific configurations investigated in this study. The mesh was created in Ansys Fluent Meshing ® by using poly-hexcore elements, and locally refined in proximity on the wing and vortex generators to ensure a good balance between computational cost and accuracy of the solution (see Fig.3). Specifically, it was ensured that at least 20 elements would be present along each dimension of the vortex generators, and that the size of the elements along the wing surface would never exceed 1% chord-length. Moreover, the boundary layer was discretised by setting the height of the first element adjacent to the wing surface wall to $2 \cdot 10^{-6}$ m, resulting in $y^+ < 1$; no inflation layer was added along the vortex vanes surfaces. The number of volumes contained in the final mesh was different across the different configuration investigated, with an average amount of about $1 \cdot 10^7$ elements.

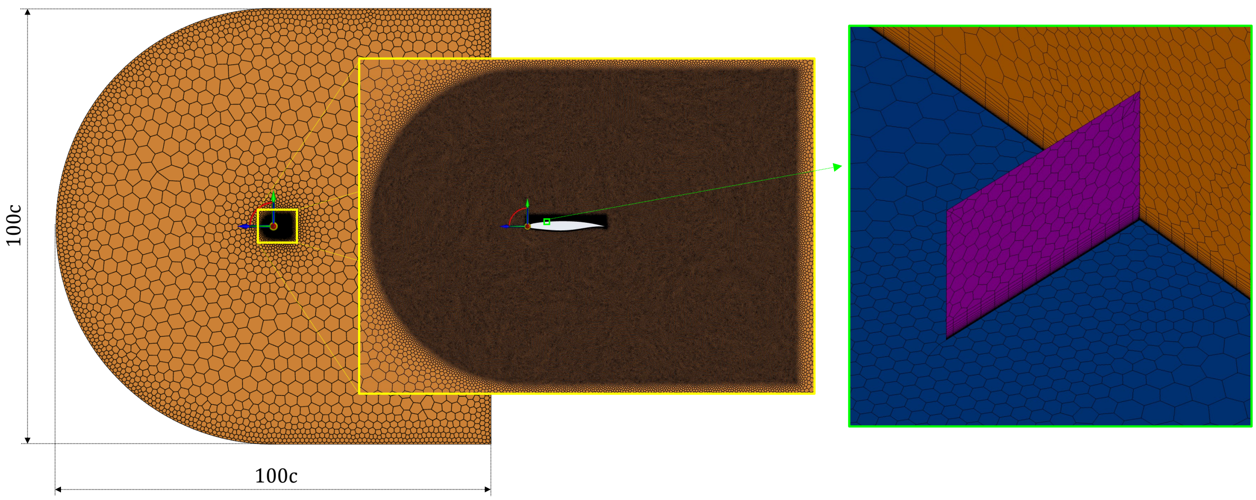

Fig. 3 Poly-hexcore mesh in the fluid computational domain, with details of the wing section and vortex vane.

CFD simulations were carried out using Ansys Fluent 3D®. The fluid domain was modelled as a compressible ideal gas, with the properties specified in Table 1. Turbulence effects were captured using the k-ω SST model [35, 36]. The CFD solver employed a pressure-based formulation with second-order spatial discretization. The simulations were executed in two stages. Initially, a steady-state analysis was performed, with convergence monitored through residuals for lift, drag, moment coefficients, and wall shear stress, requiring a threshold of $1 \cdot 10^{-5}$. If convergence was not reached within 500 iterations, the simulation was continued by transitioning to an implicit transient analysis, using the steady-state result as an initial guess, a time step of 1 ms and a maximum duration of 0.5 s.

III. Parametric investigation of a single vortex generator in cruise conditions

In this section, the aerodynamic load alleviation performance of the spoiler configuration of a single SVG is investigated for varying height and width of the vortex vane, assuming the nominal cruise conditions listed in Table 1 as flight conditions. As indicated in Fig.4, the SVG has been placed at 25% chord-length in the chord-wise direction and in the middle of the wingspan, which has been set to $2c$ to fully capture the variations in the flow distribution produced by the SVG. The parametric analysis has been carried out by means of CFD simulations, according to the methodology described in the above section, for vane heights ranging from 0.01c to 0.05c, and for vane aspect ratios between 0.25 and 10.

A. Effect on aerodynamic coefficients

Figure 5 shows the lift and drag coefficients for varying parameters h/c and w/h, compared to the clean configuration values of $C_L = 0.7217$ and $C_D = 0.0116$. The $C_L - w/h$ and $C_D - w/h$ curves show an expected results, that is, the lift alleviation and drag generation induced by the SVG always increase with the size of the vortex vane. In particular, the dependence on the vane height is consistent with the patterns observed in the two-dimensional case [3]. All the curves depicted in Fig.5 exhibit a visible transition in behaviour as the vane aspect ratio is varied, characterised by a drop in the lift coefficient and a faster increase in the generated drag. For small values of the SVG height, this transition

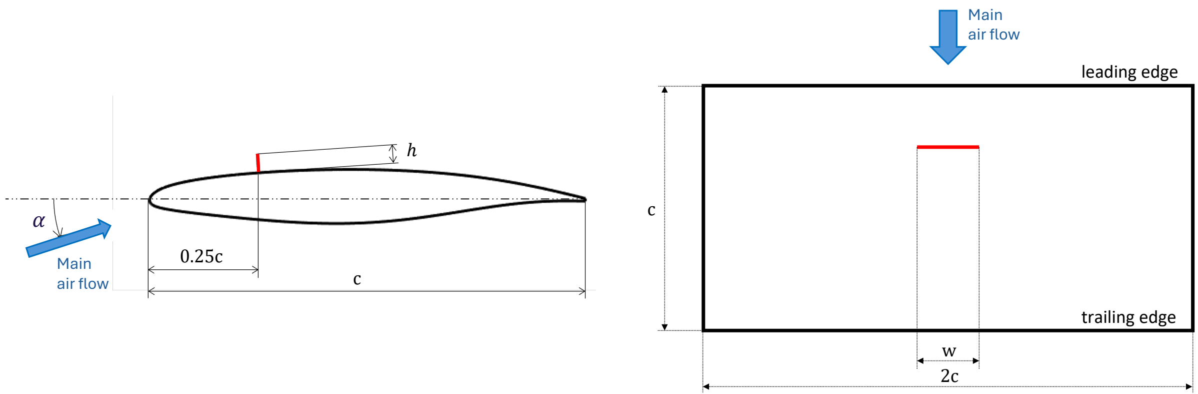

Fig. 4 Different views of the selected geometry and parameters for the single SVG analysis.

occurs smoothly and at large aspect ratios (see, e.g., the case $h/c = 0.01$). However, as the vane height increases, the C_L drop becomes sharper and occurs at lower w/h values. Therefore, it is possible to categorise the aerodynamic behaviour induced by a single SVG into two main different regimes: before the transition, only limited lift reduction and drag increase occur, particularly if shorter vanes are considered. After the transition, the C_L and C_D variation is more significant and presents an increased sensitivity to further increases of w/h. A physical explanation of this phenomenon is detailed in the following subsection.

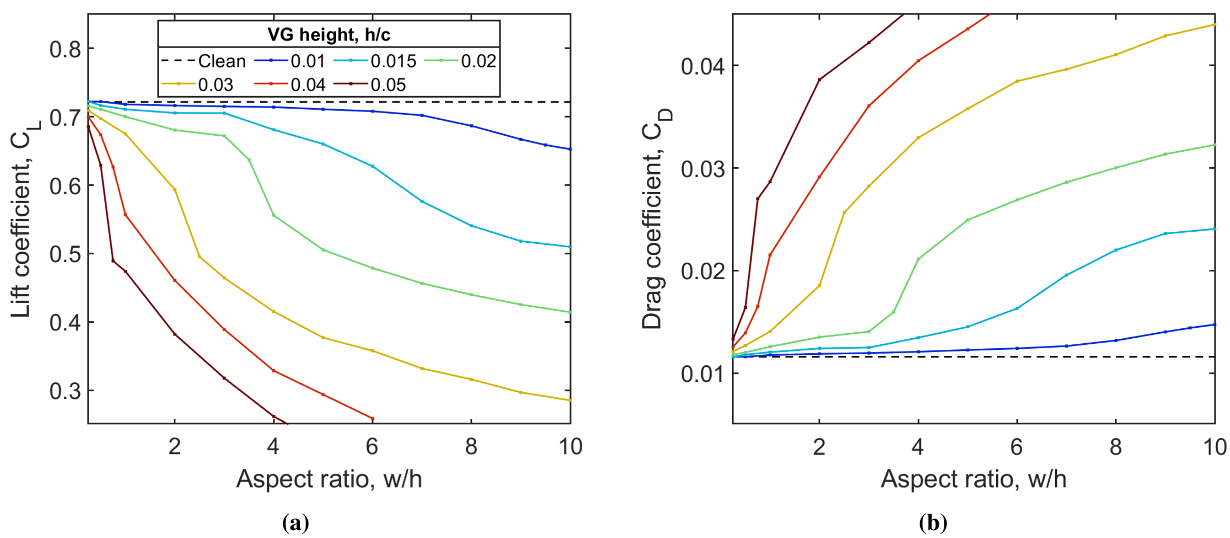

Fig. 5 Lift (a) and drag (b) coefficients in nominal cruise conditions ($\alpha = 2.15$ deg) **for varying height and width of the SVG vortex vane.**

B. Analysis of flow distribution

The effects introduced by the SVG on the flow distribution around the wing are here analysed for vortex vane height $h/c = 0.02$ and varying aspect ratio, aiming to provide further physical insight into the aerodynamic force variations addressed in the previous subsection. Figure 6 illustrates the velocity field, expressed in terms of the Mach number, around the middle section of the wing for w/h equal to 0.5, 3, 4 and 7. The corresponding pressure coefficient distributions on the upper and lower surfaces of the wing section are shown in Fig.7, along with the two-dimensional case, where the vortex vane extends over the entire wingspan. The pressure distribution for the clean wing configuration is also reported for reference. Finally, the pressure coefficient and skin friction distributions over the upper surface of the wing are depicted in Fig.8, along with the span-wise lift coefficient distribution. The results presented in these figures are discussed in what follows.

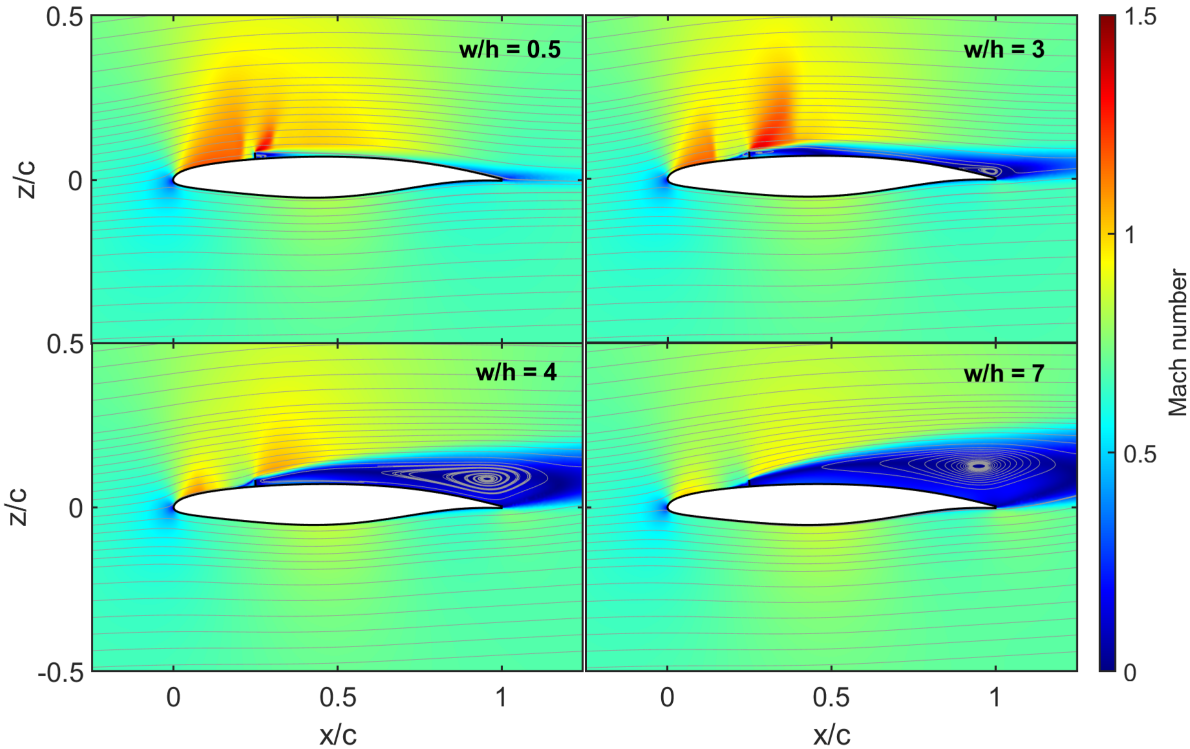

Fig. 6 Velocity field around the mid-section of the wing in cruise conditions, for $h/c = 0.02$ and varying vane aspect ratio.

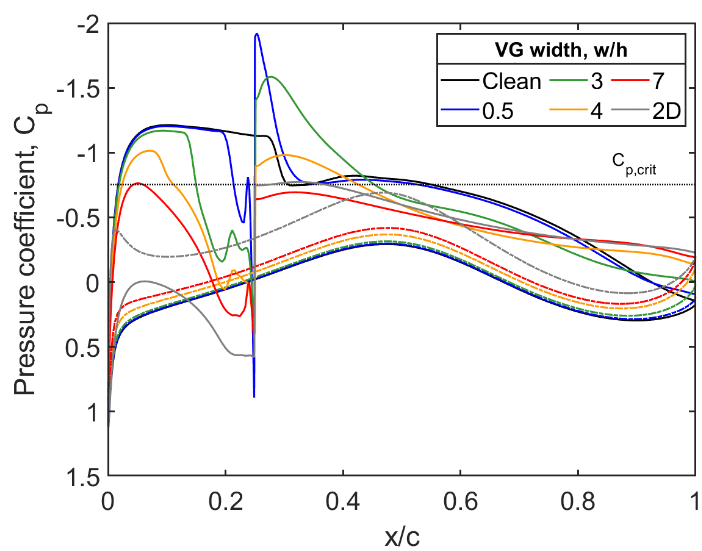

Fig. 7 Pressure coefficient distributions in the mid-section of the wing in cruise conditions, for $h/c = 0.02$ and varying vane aspect ratio.

When the aspect ratio of the vortex vane is small (see $w/h = 0.5$), the SVG has a limited impact on the velocity field around the wing. As visible in Figs.6 and 7, the device is positioned within the supersonic region of the clean wing, and only affects a small area in proximity of the of the vortex vane. In Fig.8a, a small separated region can be observed in front of the SVG, extending beyond the vortex vane in the span-wise direction, and assuming the typical shape of a

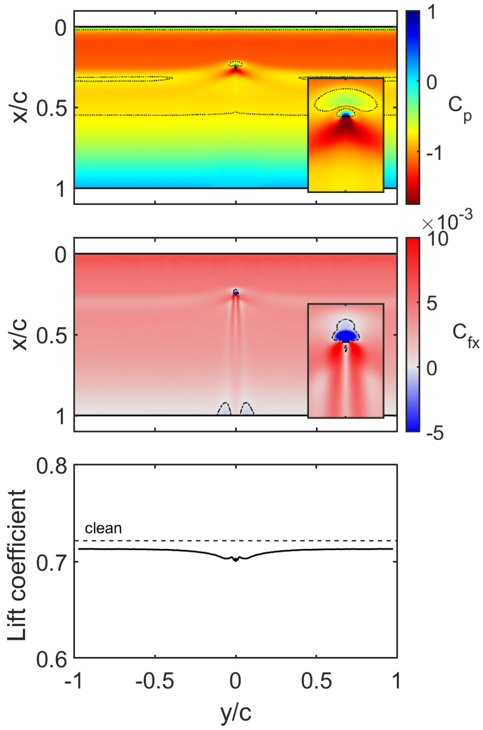

(a) $w/h = 0.5$

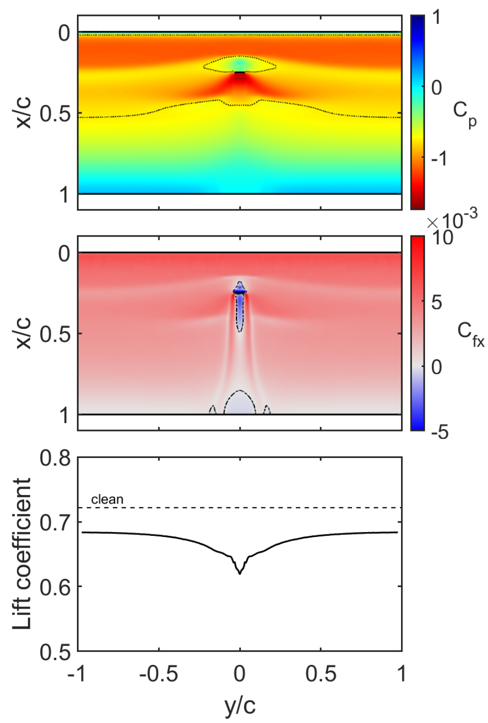

(b) $w/h = 3$

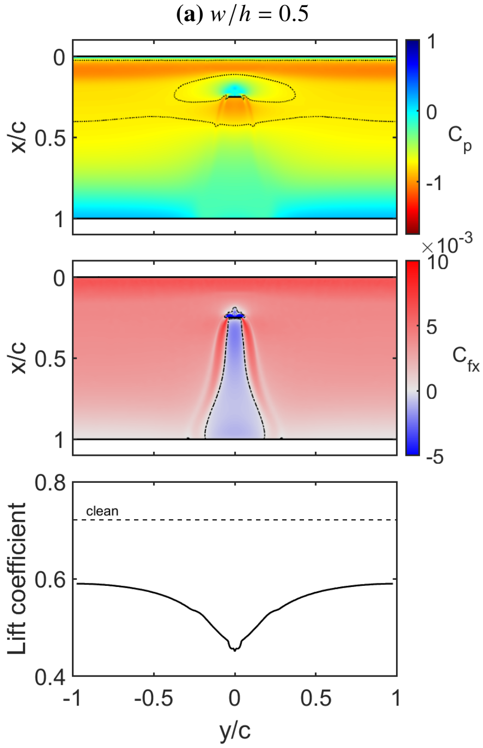

(c) $w/h = 4$

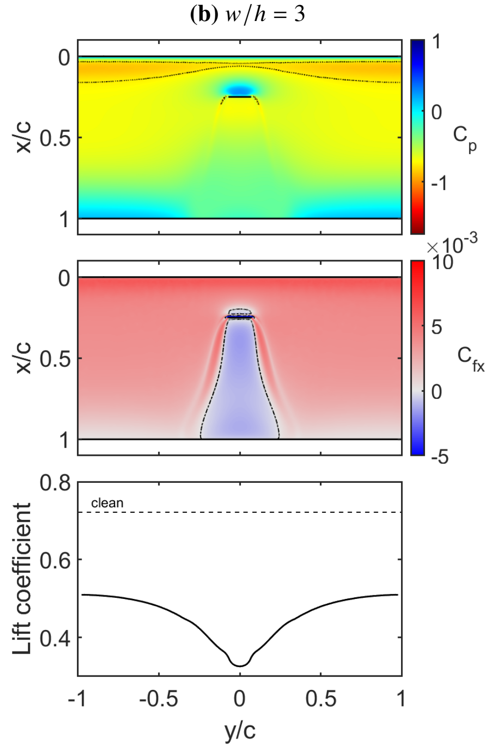

(d) $w/h = 7$

Fig. 8 Pressure, skin friction and sectional lift coefficients on the wing upper surface in cruise conditions, for $h/c = 0.02$ and varying vane aspect ratio. The dotted line shows the critical C_p, the dash-dotted line corresponds to $C_{fx} = 0$.

horseshoe vortex [37]. This region is followed by a significant pressure jump across the vane surface, characterised by a C_p variation of about 2.5 in the middle section of the wing, leading to supersonic conditions downstream. A small recirculation region can be observed in Fig.6 immediately downstream of the SVG and in proximity of the upper surface, while an expansion fan originates from the vane upper tip, leading to high local Mach number. The low pressure and high skin friction coefficient regions displayed in Fig.8a suggest that significant expansion also takes place from the side tips of the vortex vane. Only weak effects from the SVG are visible in the second half of the chord-length. The main effect in this region is the formation of two separated regions in proximity of the trailing edge, which can be identified from the $C_{fx} < 0$ areas in Fig.8a. Both regions are positioned beyond the span of the vortex vane, extending the wingspan where lift reduction due to the SVG can be observed. Nonetheless, the overall lift alleviation induced by the SVG remains negligible, due to the presence of a large pressure drop behind the vortex vane, and the lack of extensive separated regions.

As the aspect ratio of the vortex vane is increased to $w/h = 3$, some differences in behaviour can be observed. The SVG clearly divide the supersonic region located in the first portion of the chord-length into two parts. The first supersonic region terminates in a weaker normal shock-wave, followed by a subsonic region. The extension of this region, as well as of the horseshoe vortex, increases with w/h in both chord- and span-wise directions, with higher values of the pressure coefficient. The pressure drop across the vortex vane decreases in amplitude, but still leads to supersonic conditions downstream of the SVG. The low pressure-high speed region located downstream of the SVG extends in the span-wise direction for several times the span of the vortex vane, as clearly visible in Fig.8b. In the middle section of the wing, flow separation occurs up to about 50% chord-length; however, the presence of two high-speeds regions generated by the flow expansion around the side tips of the vortex vane limits the extension of the recirculation region in the span-wise direction. In proximity of the trailing edge, the flow separates once again from the upper surface, leading to a visible reduction of the sectional lift coefficient in a more significant portion of the wingspan.

As clearly visible from Figs.6 and 8, the main transition in the aerodynamic behaviour of the wing occurs (between $w/h = 3$ and 4) when the separated region downstream of the SVG extends to the trailing edge without flow reattachment. This phenomenon leads to a wide flow recirculation and a significantly larger wake, explaining the overall reduction in C_L and increase in C_D observed in Fig.5. At the trailing edge, the separated region has an extension approximately equal to three times the width of the vortex vane. Therefore, the reduction of sectional C_l becomes significant in a wide portion of the wingspan. Further increases in the SVG aspect ratio (see case $w/h = 7$) leads to a gradual disappearance of the supersonic regions and to an enlargement of the separated region, explaining the further reduction in the overall generated lift. Observing the pressure distributions obtained in the two-dimensional case in Fig.7, it is possible to deduce that the no further notable phenomena arise as the aspect ratio of the vortex vane is increased to very large values; in this case, the only visible effects are a further increase of pressure upstream of the SVG on the upper surface, and a larger flow acceleration on the lower surface. This latter aspect becomes a leading factor in the lift reduction for very large vortex vanes and can even lead to the formation of supersonic regions on the lower surface, as already observed in [3].

IV. Sensitivity analysis to variations in the angle of attack

The results presented in section III are referred to the nominal cruise conditions of the extruded wing section, corresponding to an angle of attack equal to 2.15 deg. In this section, the aerodynamic effects generated by the spoiler functionality of the SVG are investigated for varying angle of attack. The analysis is carried out in two stages, first for varying vane aspect ratio at constant height (i.e., for varying the vane width), and then for varying vane height ans fixed aspect ratio. In both cases, the chord-wise position of the SVG is fixed at 25% chord-length.

A. Effect on aerodynamic coefficients

The lift and drag coefficients curves for varying angle of attack, evaluated for: (i) $h/c = 0.02$ and varying vane aspect ratio and (ii) $w/h = 3$ and varying vane height, are represented in Figs.9 and 10. In these figures, the $C_L - \alpha$ and $C_D - \alpha$ curves evaluated for the clean configurations are also reported for reference.

In the first case, where the vane aspect ratio is varied between 1 and 5 while maintaining $h/c = 0.02$, it is possible to observe from Fig.9 that the effect of the SVG is minimal at small or negative incidence. However, as the angle of attack is increased, a transition occurs in each curve, after which lift reduction and drag increase become more significant. For large SVGs (see cases $w/h = 4$ and 5), this transition occurs at small angles of attack, lower than 2.15 deg. This is consistent with the behaviour illustrated for cruise conditions in Fig.5, where it can be observed that, for $h/c = 0.02$, these two values of the aspect ratio are located after the transition from partial to full flow separation. In full separation regime, the slope of the $C_L - \alpha$ curves is strongly reduced by large SVGs, determining a limited variation of C_L for increasing α. At high angles of attack, it is visible that stall occurrence is significantly delayed by large SVGs, and characterised by a lower C_L value. SVGs with intermediate aspect ratios (see $w/h = 3$) lead to similar overall patterns in the $C_L - \alpha$ curves; however, in this case, the transition from partial to full separation regimes occurs very smoothly and with a lower drag increase. Low-aspect ratio SVGs (see $w/h = 1$ and 2) offer a less desirable behaviour for varying α. Besides leading to a negligible lift reduction at small angles of attack and in cruise conditions, they exhibit sudden variations in lift when α is increased. This peculiar behaviour is due to the occurrence of transonic phenomena, as explained in detail in Sect.IV.B.

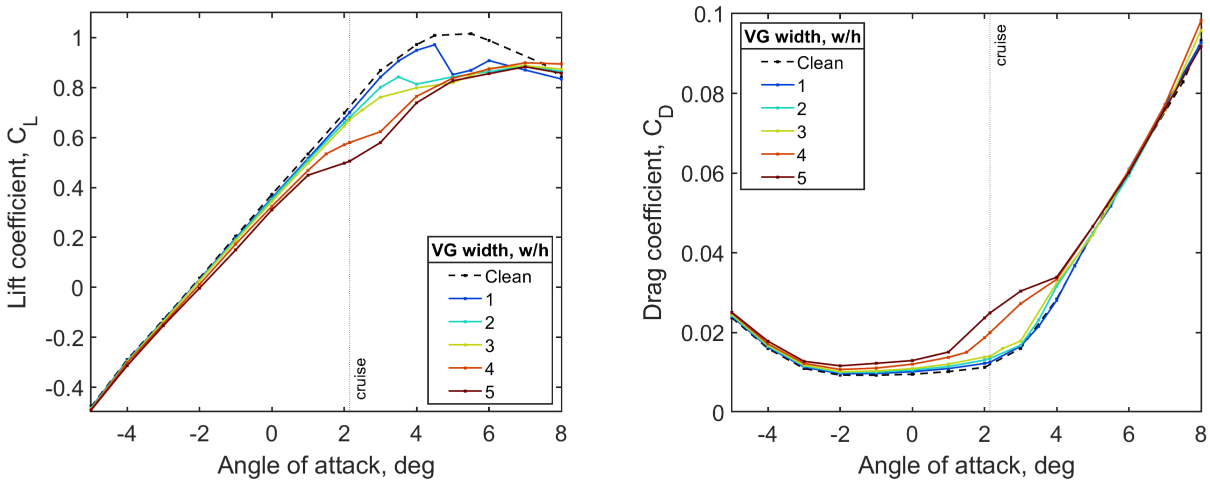

(a) (b)

Fig. 9 Lift (a) and drag (b) coefficients vs angle of attack, for $h/c = 0.02$ and varying vane aspect ratio.

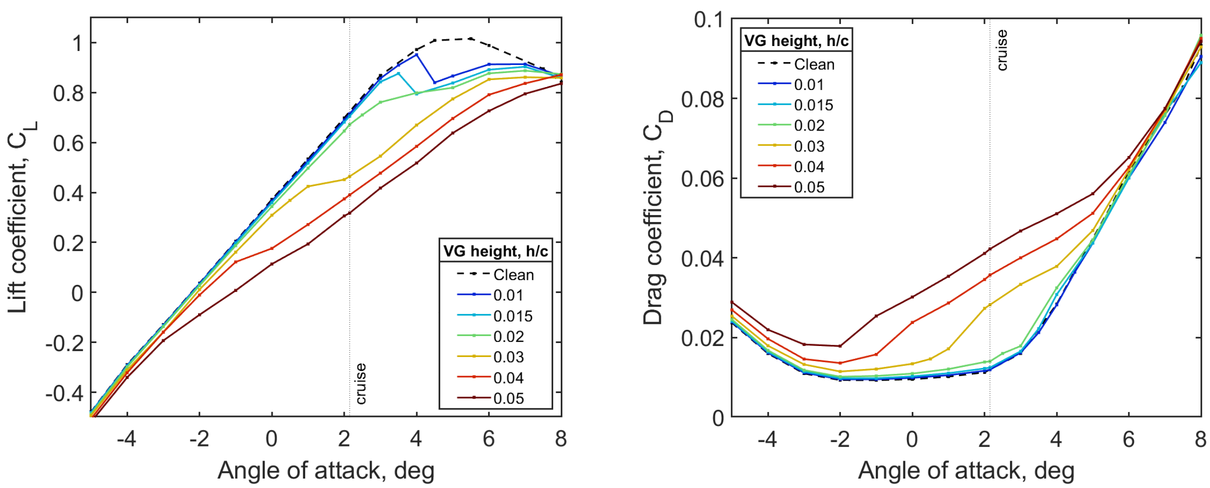

(a) (b)

Fig. 10 Lift (a) and drag (b) coefficients vs angle of attack, for $w/h = 3$ and varying vane height.

Fig.10 shows the lift and drag coefficient variation with the angle of attack, for fixed vane aspect ratio and varying height between $0.01c$ and $0.05c$. Although these curves present similar patterns to those observed in Fig.9, it is also visible that the vortex vane height has a stronger impact on the SVG performances than its width. SVGs generally have little effect on the aerodynamic forces at large negative incidence; however, higher SVGs (see $h/c = 0.04$ and 0.05) can trigger full flow separation even for negative values of α. After the transition from partial to full flow separation, the lift coefficient increases with the angle of attack at a reduced slope with respect to the clean wing, maintaining a linear pattern in a wide range of α and delaying the stall occurrence; similarly, the $C_D - \alpha$ curve also shows a linearly increasing pattern for most values of the angle of attack. The lift and drag coefficient curves in Fig.9 are qualitatively similar to those obtained in [3] for varying SVG height in two-dimensional flow conditions, although the finite vane span leads to a more limited C_L reduction in the present analysis. Shorter SVGs (see, e.g., $h/c = 0.01$ and 0.015) present more complex patterns, with appreciable lift reduction only taking place in proximity of the stall of the clean wing. This behaviour is similar to that exhibited by low-aspect ratio SVGs and will be discussed in the following subsection.

B. Analysis of flow distribution

In this subsection, the effect introduced by a SVG on the velocity field around the wing, and on the pressure and skin friction distributions on the upper surface, is discussed for varying angle of attack in two different configurations, i.e., for $w/h = 3$ and $w/h = 1$. In both cases, the vane height is set at $h/c = 0.02$.

The $C_L - \alpha$ and $C_D - \alpha$ curves for $w/h = 3$ and $h/c = 0.02$ are illustrated in both Figs.9 and 10, where it is possible to observe that this SVG configuration produces similar patterns to those exhibited by larger devices. To establish the physical causes of this type of behaviour, the velocity field around the middle section of the wing is illustrated in Fig.11 for angle of attack equal to -4, 1 and 4 degrees. In addition, the corresponding pressure and skin friction coefficients distributions are represented in Fig.12, along with the span-wise C_l distribution. In the case $\alpha = -4$ deg, it can be observed that the SVG is not able to trigger any significant flow separation. The flow reattaches to the upper surface immediately downstream of the vortex vane, and only two very small separated regions are visible at the trailing edge. Therefore, sectional lift reduction is only achieved within the wingspan fraction occupied by the SVG, and its value is overall negligible. As the angle of attack is increased to 1 degree, a larger recirculation area can be observed downstream of the SVG and expansion around the top and side tips of the vortex vane is such to generate supersonic conditions; a further supersonic region is also visible in proximity of the leading edge. Moreover, the extension and number of separated regions at the trailing edge increases, leading to a more significant overall lift reduction. Further increases in the angle of attack lead to drastic changes in the aerodynamic behaviour. At $\alpha = 4$ deg, the flow has already transitioned to a full separation regime. A large recirculation region can be observed downstream of the SVG becomes, followed by a large wake. As discussed in Sect.III, full flow separation leads to a major reduction in the lift produced by the wing. It is also worthwhile mentioning that, as α is increased, the two supersonic regions observed for $\alpha = 1$ deg eventually merge and move upstream of the SVG. At higher incidence, the SVG becomes fully immersed in separated region originating from the shock-induced separation, leading to a gradual loss of its effectiveness.

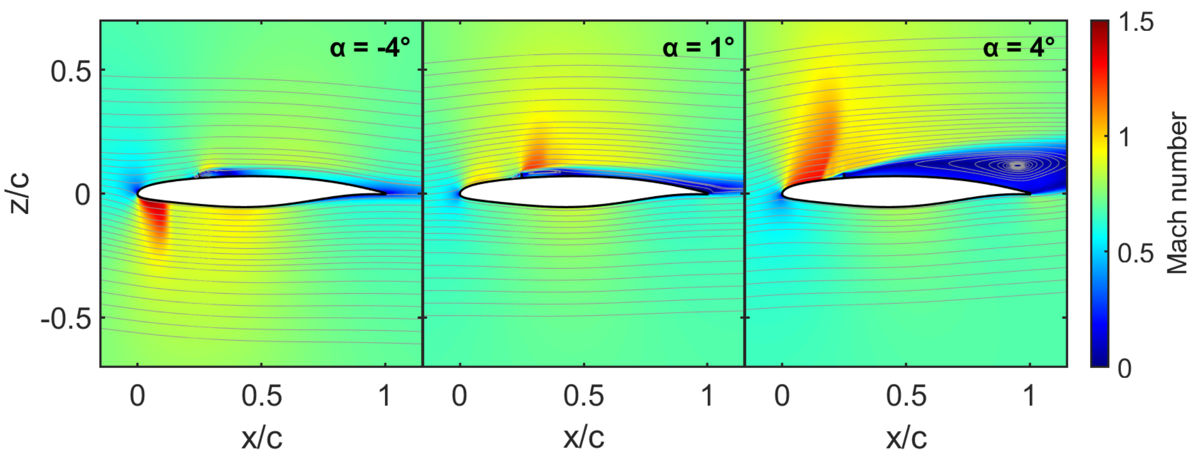

Fig. 11 Velocity field around the mid-section of the wing, for $h/c = 0.02$, $w/h = 3$ and varying angle of attack.

To explore the behaviour of smaller SVGs, characterised by small height and/or aspect ratio, the case $w/h = 1$ and $h/c = 0.02$ is now considered. The velocity field around the wing and the pressure and skin friction distributions over the upper surface are displayed in Figs.13 and 14 respectively, for the cases $\alpha = 4$, 4.5, 5 and 8 degrees. The case $\alpha = 4$ deg is representative of the aerodynamic behaviour induced by the SVG before the transition from partial to full flow separation (see the blue curve in Fig.9a). The SVG falls entirely within the supersonic region located at the front of the wing, leading to an oblique shock-wave upstream and to an expansion fan around the upper tip of the vane. The patterns introduced downstream of the SVG are quite complex: in the middle section of the wing (Fig.13) , the normal

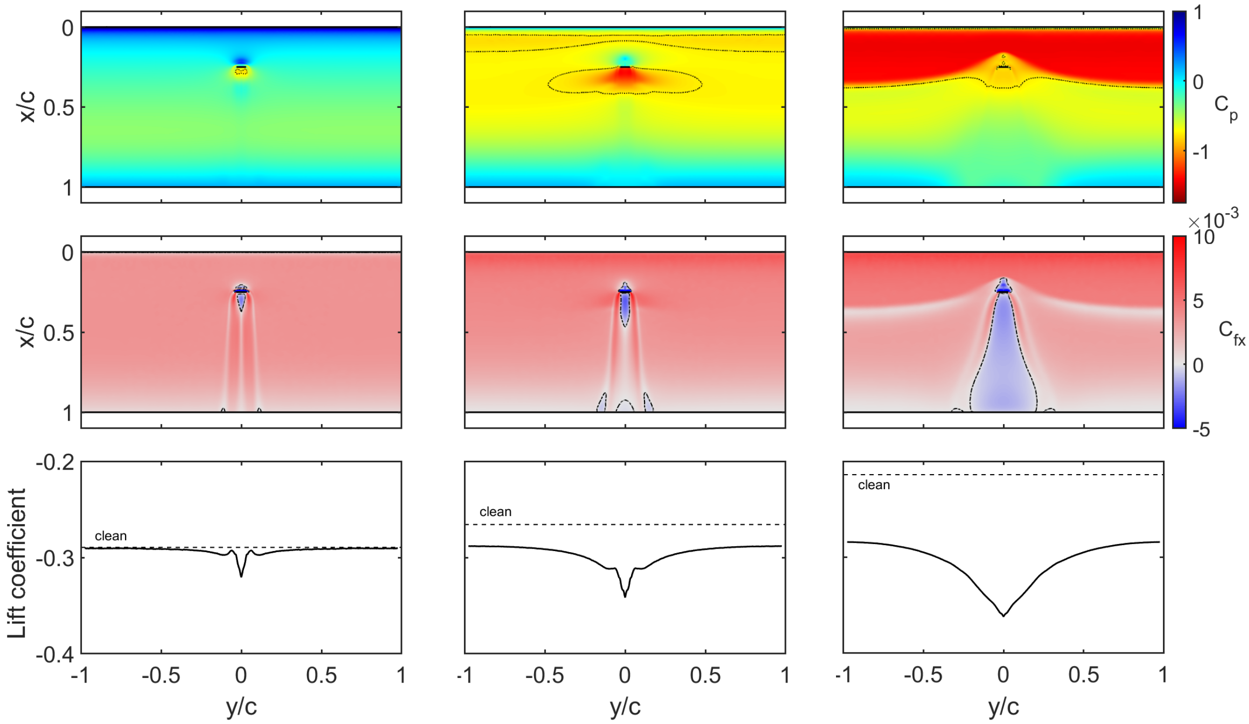

(a) $\alpha = -4$ deg **(b)** $\alpha = 1$ deg **(c)** $\alpha = 4$ deg

Fig. 12 Pressure, skin friction and sectional lift coefficients on the wing upper surface for $h/c = 0.02$, $w/h = 3$ and varying angle of attack. The dotted line shows the critical C_p, the dash-dotted line corresponds to $C_{fx} = 0$.

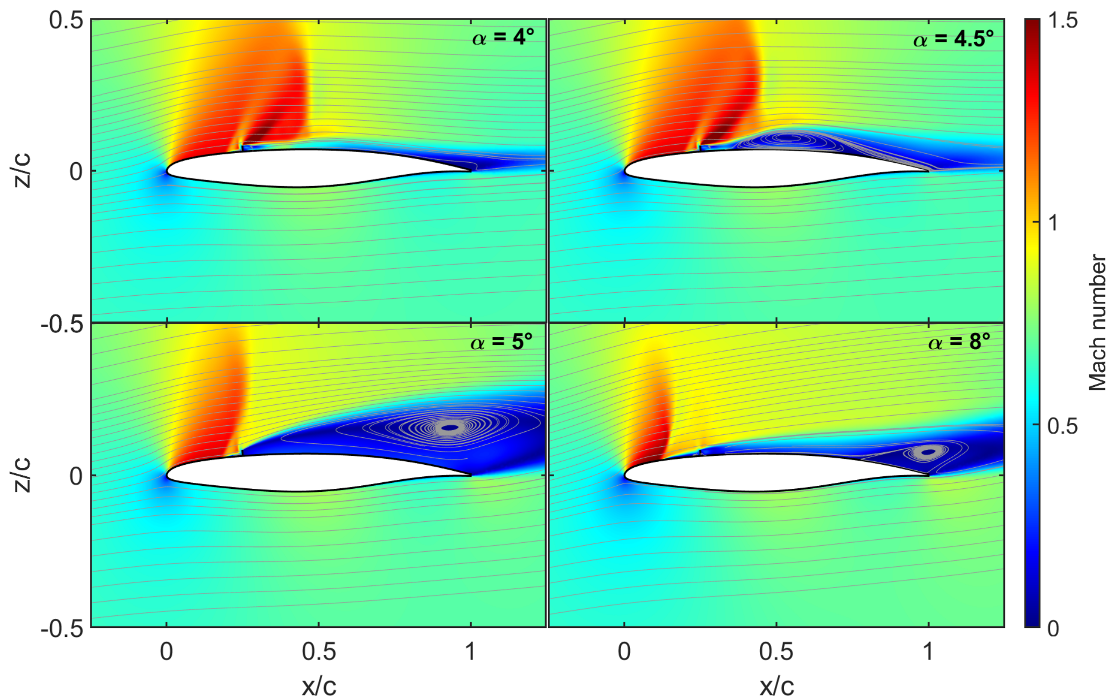

Fig. 13 Velocity field around the mid-section of the wing, for $h/c = 0.02$, $w/h = 1$ and varying angle of attack.

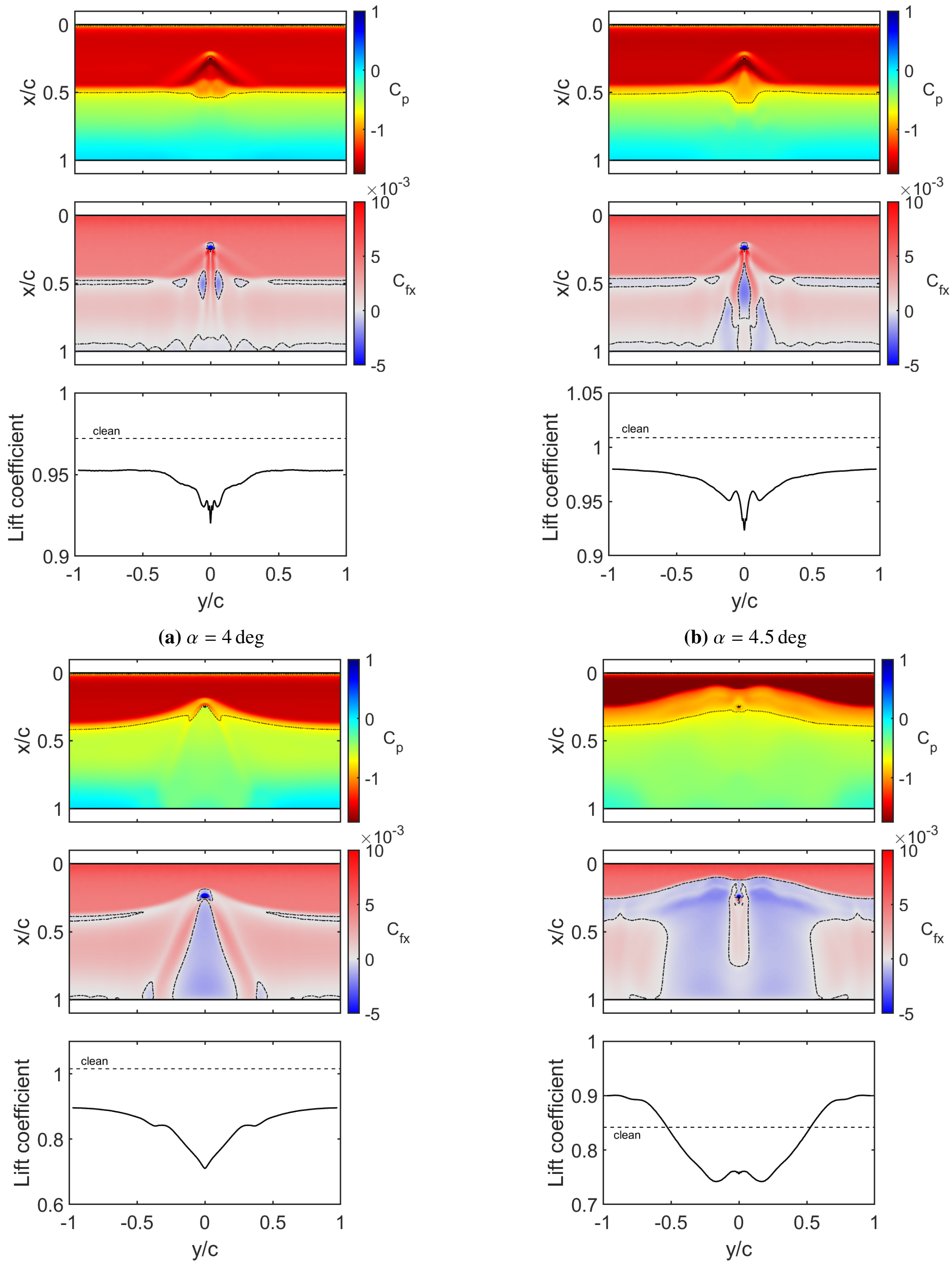

(a) α = 4 deg

(b) α = 4.5 deg

(c) α = 5 deg

(d) α = 8 deg

Fig. 14 Pressure, skin friction and sectional lift coefficients on the wing upper surface for $h/c = 0.02$, $w/h = 1$ and varying angle of attack. The dotted line shows the critical C_p, the dash-dotted line corresponds to $C_{fx} = 0$.

shock-wave delimiting the supersonic region does not reach the upper surface of the wing, but Fig.14a reveals that flow separation occurs in two lateral areas located further downstream. In addition, the SVG disrupts the shock-induced separation pattern observed in the clean wing configuration, and alters the flow separation occurring in proximity of the trailing edge. The overall effect is a very limited lift reduction, spread rather uniformly along the wingspan. A small increase in the angle of attack leads to a very different scenario. In the case $\alpha = 4.5$ deg, a large recirculation region appears downstream of the SVG (see Fig.13), determining a sudden increase in pressure on the upper surface and, consequently, a reduction in the overall lift. Separated regions also visibly enlarge in other areas of the wing upper surface, as shown in Fig.14b. When $\alpha = 5$ deg, full separation eventually occurs downstream of the SVG, leading to an extensive recirculation region and a large wake. Figure 14c shows how the different separated regions observed for $\alpha = 4.5$ deg eventually merge into the main SVG wake. The supersonic region ends in a normal shock-wave, upstream of the SVG along the vane span, and positioned at about 40% chord-length far away from the SVG. If the angle of attack is further increased, the normal shock-wave moves closer to the leading edge, with shock-induced separation extending to most of the wing upper surface, as visible in Fig.14d for $\alpha = 8$ deg. In this case, the presence of the SVG can enforce the reattachment of the flow downstream, particularly in regions further away from the SVG itself, and the sectional lift coefficient can become locally higher than in the clean wing configuration, resulting in a negligible (or negative) overall load alleviation.

V. Parametric investigation of multiple vortex generators in cruise conditions

This section focuses on the analysis of the load alleviation performance provided by multiple SVGs, operated in their spoiler configuration, placed on the wing upper surface at 25% chord-length and spaced equidistantly in the span-wise direction. For simplicity, the value of the vortex vane height is fixed at $h/c = 0.02$ in the current investigation. The analysis is conducted in two steps. Firstly, the interaction between two identical SVGs is studied for varying aspect ratio w/h and normalised distance Δ/h between the rotation axes. In this case, as shown in Fig.15a, the portion of wingspan analysed is limited to the distance Δ, so that the SVG axes are located on the boundaries of the computational domain in the span-wise direction, where symmetry boundary conditions are imposed. In the second step, the analysis is extended to the case where multiple identical SVGs are placed on a straight wing of fixed length equal to c (see Fig.15b), while the number N of SVGs employed is varied along with aspect ratio of their vanes. Also in this case, the rotation axes of the two most external SVGs are placed in correspondence of the computational domain side boundaries, where symmetry conditions are enforced.

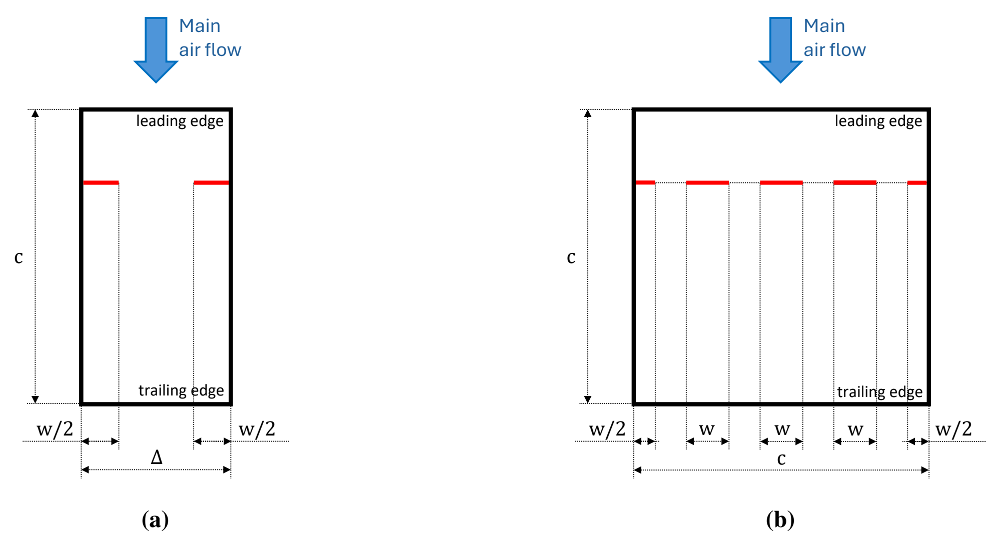

Fig. 15 Wing geometries analysed for: (a) interaction between two SVGs placed at a distance Δ, and (b) interaction among N SVGs placed on a wingspan of length c.

In both analyses, a further parameter is considered to facilitate the comparison among different configurations. Let us introduce the *wall ratio* as

$$\phi = \frac{w}{\Delta}, \tag{1}$$

i.e., as the ratio between the vortex vane width and the distance between two SVGs' rotation axes. When a series of SVGs is used to perform load alleviation on a given wingspan, the wall ratio corresponds to the overall fraction of wingspan occupied by the vortex vanes (in spoiler configuration). If the given wingspan is equal to c, as in Fig.15b, then:

$$\phi = \frac{Nw}{c}. \tag{2}$$

A. Interaction between two SVGs

CFD simulations have been carried out, according to the methodology described in Sect.II, for the geometry illustrated in Fig.15a, considering different aspect ratios between 1 and 5, and for varying wall ratios between 0 and 1. In particular, the limit case $\phi = 1$ corresponds to that of a spoiler extending over the entire wingspan, while $\phi = 0$ is representative of the clean configuration of the wing.

The lift and drag coefficient resulting from the simulations are represented in Figs.16a and b respectively, as functions of the wall ratio, and for varying aspect ratios. It is possible to observe that, as expected, lift reduction and drag generation both increase when the wall ratio is increased, i.e., when the distance between the two SVGs is reduced. However, the patterns followed by these curves can strongly vary depending on the vanes aspect ratio, highlighting how, due to the complexity of the interactions between SVGs, this parameter can become crucial to obtain better load alleviation performances. At low values of the wall ratio parameter, when the distance between the SVGs is still large, the largest lift reduction is obtained by employing large vortex vanes. However, this behaviour is inverted for high values of the wall ratio, where low aspect ratio devices deliver best performances for lift alleviation. The drag coefficient curves tend to follow a similar pattern, with maximum drag produced by larger SVGs at low wall ratios, and by SVGs with low aspect ratio at higher wall ratios. However, it is noteworthy that the minimum generated drag at either low or high wall ratios is obtained for w/h, which is an intermediate value in the investigated range of aspect ratios.

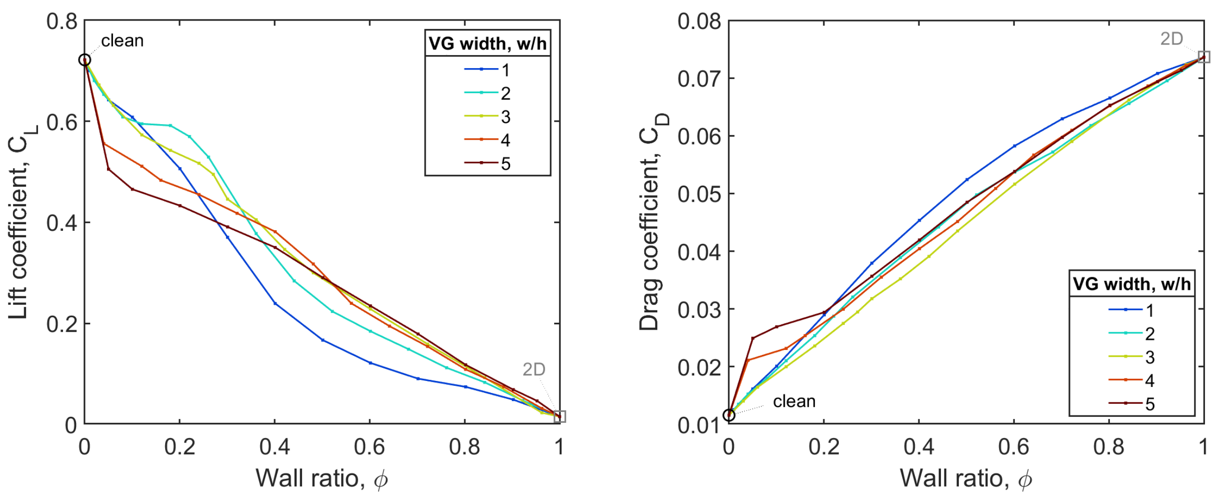

(a) (b)

Fig. 16 Lift (a) and drag (b) coefficients in nominal cruise conditions ($\alpha = 2.15$ deg) for $h/c = 0.02$, and varying wall ratio and vane aspect ratio of two SVGs.

The pressure and skin friction variations at different distances between the rotation axes provide further insight into the aerodynamic forces generated by two SVGs. Let us first take into exam the case of $w/h = 3$, for which the pressure and skin friction coefficient distributions on the upper surface are illustrated in Fig.17. For low wall ratio (see $\phi = 0.06$), the interaction between the SVGs is minimal and the patterns displayed by pressure and skin friction coefficients closely recall those observed in the analogous single VG case, in Fig.8b, with small separated regions visible immediately downstream of the SVGs, and further ones appearing near the trailing edge. Subsonic regions can also be observed upstream of each SVG, indicating the presence of disconnected horseshoe vortices. As it is possible to observe in Fig.16, the lift reduction and drag increase are very close to twice the variations obtained from a single SVG, further proving the limited extent of the interaction. As the wall ratio is increased, the interaction between the SVGs starts building up. At $\phi = 0.12$, the horseshoe vortices of the SVGs merge, splitting the supersonic region into two separate regions. At

$\phi = 0.3$, it can be seen that the separated regions downstream of the SVGs are significantly enlarged, while recirculation areas on the trailing edge merge into a single one, placed between the SVG. The increased extent of flow separation results in a stronger overall lift reduction, despite the interaction between the SVGs also produces a significant suction peak in the middle section of the wing, downstream of the vortex vanes line. As the wall ratio is increased to 0.48, it is possible to observe a loss of symmetry in the flow distribution on the upper wing. The separated region downstream of one of the SVGs enlarges significantly, altering the pressure and skin friction distributions, and resulting in a reduction in size of the separated region of the other SVG. In this condition, it can also be seen that supersonic conditions are no longer reached upstream of the SVGs, while they are still visible downstream of the vanes line. Further increases in the wall ratio result in a further extension of the separated region, which eventually covers the entire wing portion located downstream of the SVGs line. In this case (displayed for $\phi = 0.96$), the lift reduction performance become very similar to that provided by a single spoiler covering the entire wingspan.

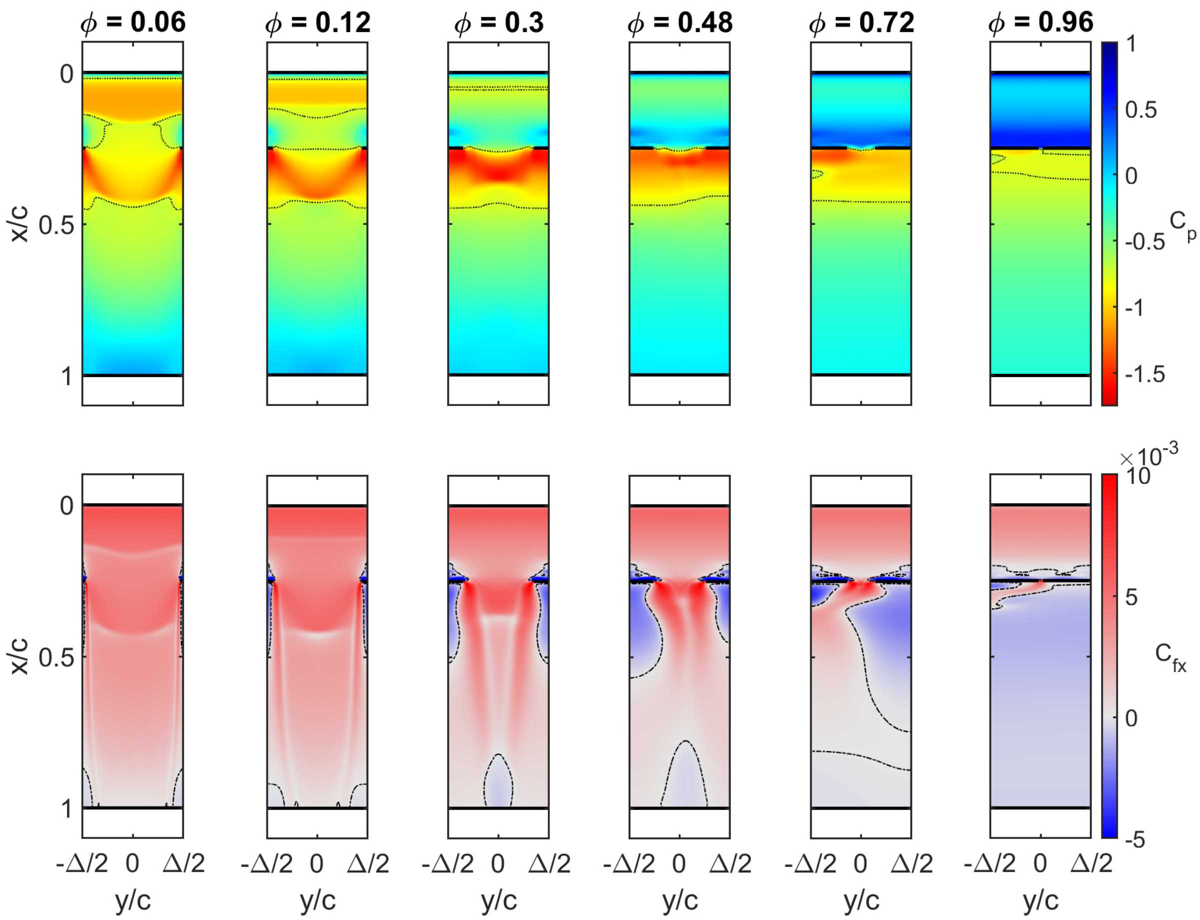

Fig. 17 Pressure and skin friction coefficients on the upper surface for $h/c = 0.02$, $w/h = 3$ and varying wall ratio. The dotted line shows the critical C_p, the dash-dotted line corresponds to $C_{fx} = 0$.

While the case $w/h = 3$ addresses most of the fundamental features of the interaction between two SVGs, further aerodynamic phenomena can take place when different aspect ratios are considered. The most peculiar pattern among the $C_L - \phi$ curves in Fig.16 is exhibited by the case $w/h = 2$, where the lift coefficient remains approximately constant in the wall ratio range included between 0.1 and 0.2, meaning that the interaction between closer SVGs heavily affects their lift alleviation performance in this interval. The pressure and skin friction distributions on the wing upper surface are represented in Fig.18a for varying ϕ between 0.12 and 0.26. Observing the cases $\phi = 0.12$ and $\phi = 0.18$, it is possible to deduce that the generated lift remains very similar in these two cases due to the superposition of different physical phenomena. The leading phenomenon responsible for the poor load alleviation performances observed for $\phi = 0.18$ is the strong suction peak generated by the interaction between the SVGs in the mid-section of the wing. In the case $\phi = 0.3$ of Fig.17, the effects of a similar suction peak were fully compensated by the increasing extension of the separated regions downstream of the SVGs, and at the trailing edge. However, for $w/h = 2$ and $\phi = 0.18$, separated regions remain very similar to those observed for $\phi = 0.12$, with the high-speed region even enforcing flow reattachment downstream of the devices. All these effects fully counterbalance the lift decrease resulting, in comparison with the case $\phi = 0.12$, by the reduction of the extent and intensity of the supersonic region located near the leading edge, eventually leading to a similar C_L in these two configurations. For $\phi = 0.22$ and $\phi = 0.26$, in Fig.18a, the extension of the high-speed region downstream of SVGs line progressively reduce, and a more significant flow separation takes place at the trailing edge, contributing to the gradual lift coefficient diminution observed in Fig.16a for $\phi > 0.2$.

In Fig.16a, it is noteworthy that, for $w/h \geq 4$, lift and drag coefficient curves present a different pattern for low wall ratios. A straightforward explanation of this behaviour is that, as shown in Sect.III, these SVGs are able to trigger full flow separation in cruise conditions even without interacting with other devices. Nonetheless, in Fig.18b, it can be observed that, for $w/h = 4$, the interaction between SVGs at small distances can re-energise the flow downstream of the SVGs line and result in a partial reattachment downstream of each vortex vane, reducing the load alleviation performance at low wall ratios. The same phenomenon is only partly observed for $w/h = 5$, in Fig.18c. In this case, the interaction does not result in a reattachment of the flow downstream of the SVGs, but can still alter the flow distribution, introducing notable asymmetries even at small values of ϕ, while for aspect ratios $w/h < 5$ asymmetric flow distributions on the upper surfaces have only been observed starting from $\phi \cong 0.4$.

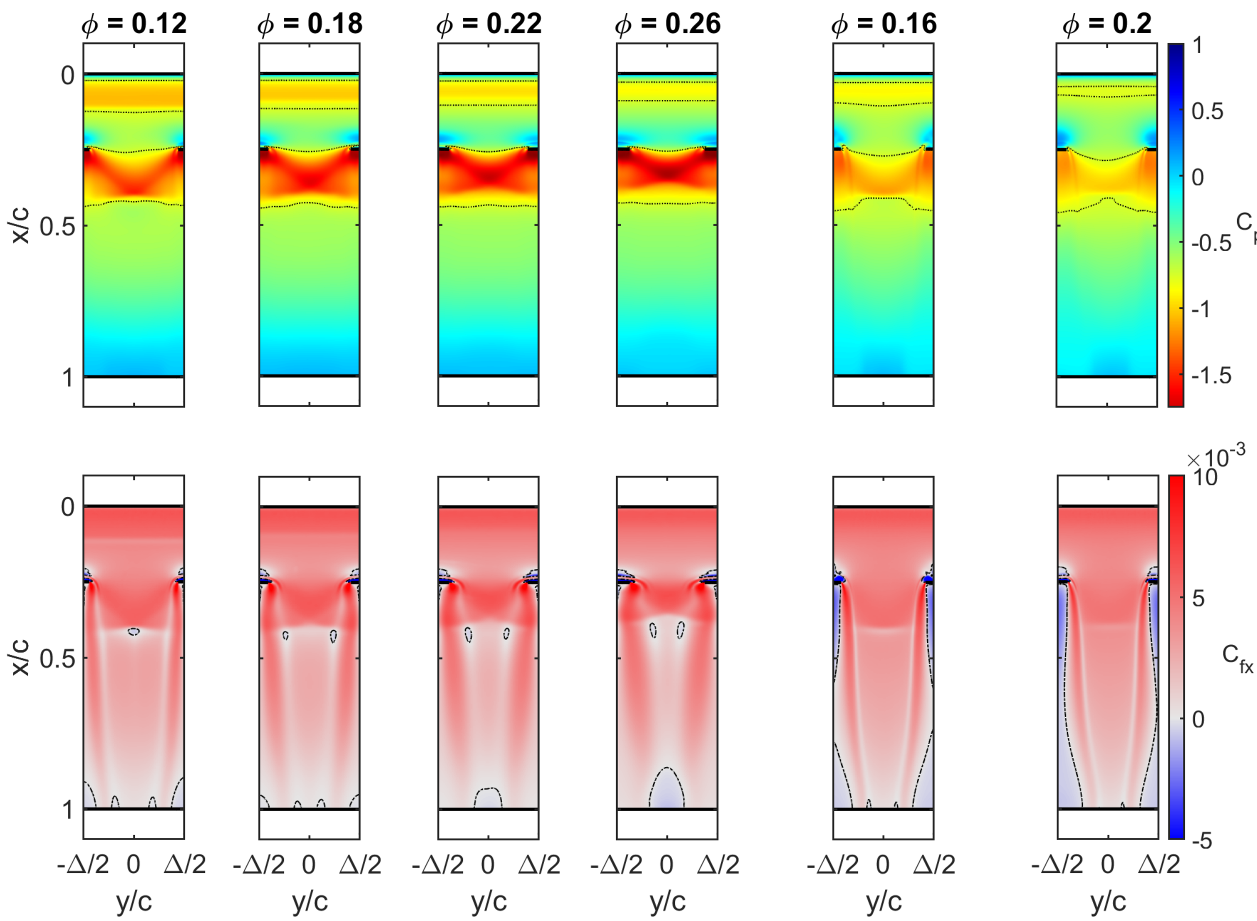

(a) $w/h = 2$ **(b)** $w/h = 4$ **(c)** $w/h = 5$

Fig. 18 Pressure and skin friction coefficients on the upper surface for $h/c = 0.02$, and varying aspect and wall ratios. The dotted line shows the critical C_p, the dash-dotted line corresponds to $C_{fx} = 0$.

B. Interaction among multiple SVGs

The load alleviation performance provided by a series of identical SVGs placed on an assigned wingspan has been investigated by carrying out CFD simulations on the geometry represented in Fig.15b for varying aspect ratio and number of SVGs, resulting in different values of the wall ratio, according to Eq.(2).

The lift coefficient-wall ratio curves obtained for each value of w/h, between 1 and 5, are compared to those derived in the previous investigation in Fig.19, where it is possible to observe a good overall agreement. This agreement proves that the results presented in subsection V.A provide an overall realistic description of how the aspect and wall ratio parameters can affect the lift reduction performance provided by multiple SVGs. Nonetheless, a few discrepancies can be observed in the comparison, and are further discussed in what follows.

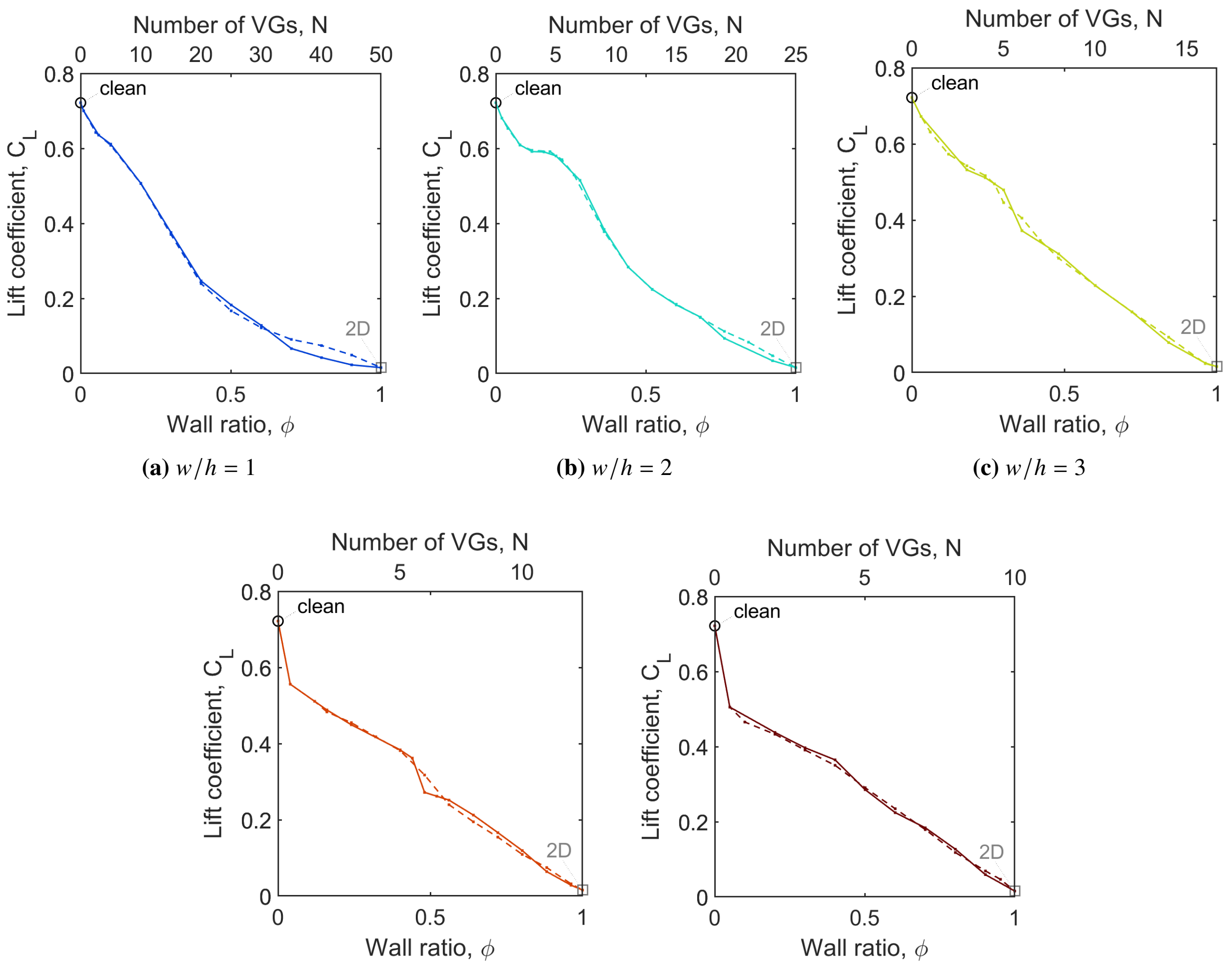

(a) $w/h = 1$ **(b)** $w/h = 2$ **(c)** $w/h = 3$ **(d)** $w/h = 4$ **(e)** $w/h = 5$

Fig. 19 Comparison of lift coefficient curves evaluated for $h/c = 0.02$ by using two or multiple VGs at a given wall ratio.

The main range of disagreement between the two investigated cases is observed for wall ratios above 0.7, particularly in the case of low aspect ratio values (see $w/h = 1$ and $w/h = 2$). Figure 20a represents a comparison between the results obtained for $w/h = 1$ and $\phi = 0.8$ by taking into account the geometries from Figs.15 a and b respectively. It is possible to observe how the interaction among several SVGs, in very packed configurations, contribute to the creation of a very uniform flow separation over the entire wing upper surface downstream of the vortex vanes. This effect further enhances the load alleviation provided by the set of SVGs, whose performance becomes very close to that of a continuous spoiler extending over the entire wingspan.

In general, discrepancies between the C_L curves appear for those configurations where asymmetry has been observed in the two-SVGs investigation. In particular, in the cases $w/h = 3$ and $w/h = 4$, the main disagreement is observed around $\phi = 0.4$, where, as previously mentioned, asymmetries first appears in the flow distribution over the wing upper surface. A comparison between the results obtained by the two different approaches is achieved in Fig.20b for the case $w/h = 4$ and $\phi = 0.48$. It can be seen that, in the presence of the asymmetric pattern displayed for the two-SVGs case, the flow distribution can significantly differ when multiple SVGs are considered. In fact, for these values of the aspect and wall ratios, full flow separation is incumbent for all the SVGs and may first occur downstream of any of them; in the multiple-SVGs case of Fig.20b, full separation only takes place downstream of the third SVG. When this happens, the flow distribution around the remaining devices is strongly altered, often preventing full flow separation downstream of the other SVGs. From a mathematical perspective, this suggests the presence of multiple solutions, for the given flow condition and SVGs parameters, when the system's response loses its periodicity, leading to an uncertainty in the expected lift reduction. Further numerical and experimental research will be needed to assess if the cause of this phenomenon resides in the nonlinear nature of the problem, or can be due to limitations in the methodology used in the present investigation.

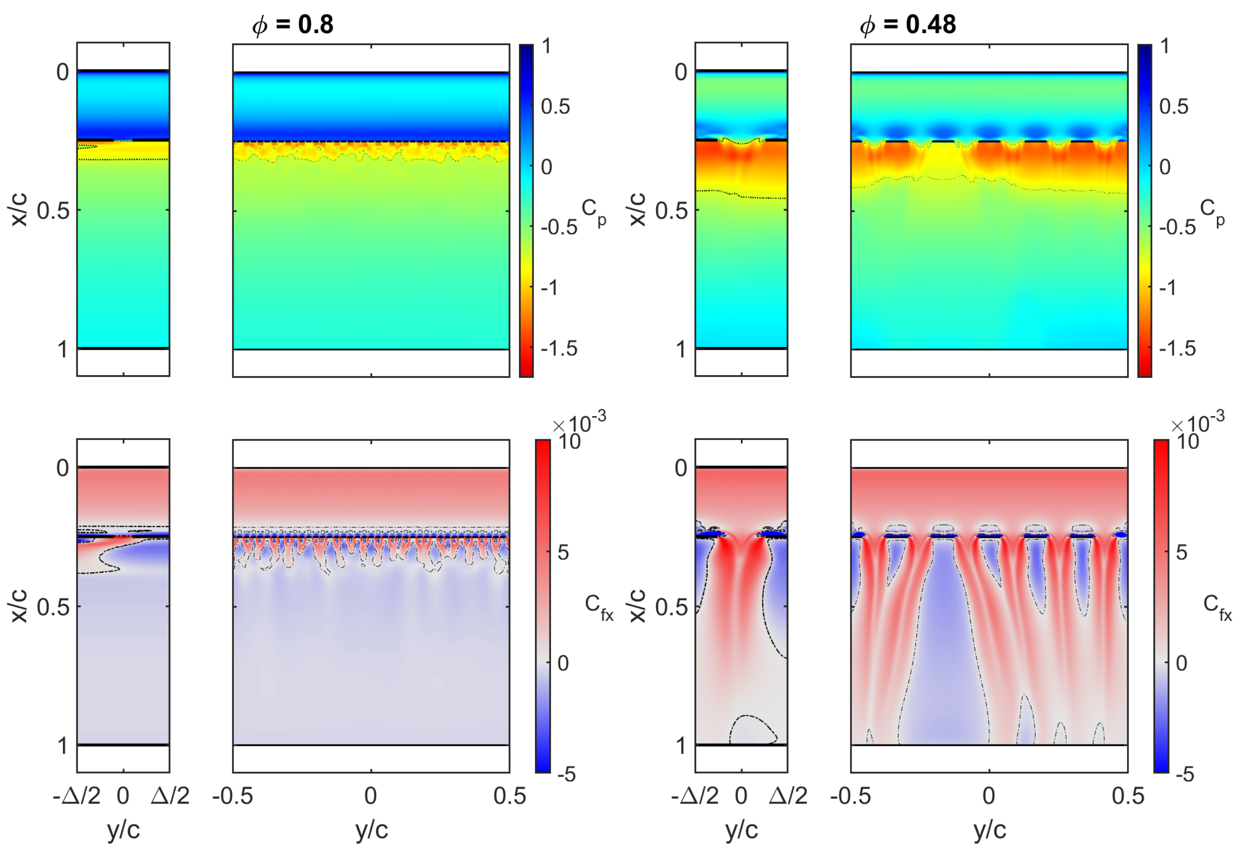

(a) $w/h = 1$

(b) $w/h = 4$

Fig. 20 Comparison between pressure and skin friction coefficients on the upper surface evaluated for $h/c = 0.02$ by using two or multiple VGs at a given wall ratio.

C. Discussion

The results presented in this section, along with those previously derived for the case of a single SVG, provide useful information for the design and selection of finite-span spoiler devices for load alleviation purposes. Possible criteria for parameter selection are therefore analysed in the following discussion.

The main design requirement for SVGs in spoiler configuration is to yield the desired lift reduction over a given portion of the wingspan in high-speed conditions. As showed in Fig.16a, for a given vortex vane height, the same lift reduction can be achieved by considering multiple combinations of the aspect and wall ratio parameters; therefore, further criteria might be considered to determine the optimal parameter selection for the intended purposes. While drag increase is generally unavoidable when performing load alleviation with mechanical devices such as mini-tabs, which operate by triggering flow separation, it is also desirable to maintain the C_D as low as possible. Fig.21 displays the drag increase associated with the achieved lift reduction for different vortex vane aspect ratios. From these results, it appears clear that the optimal aspect ratio varies according to the required lift reduction. If only a limited lift reduction is needed ($\Delta C_L \leq 0.3$), large aspect ratio devices should be preferred as they generate less additional drag. In fact, when their mutual distance is relatively large, indicatively between 3 and 10 times the vane width in the investigated case-study, the interaction between low-aspect ratio SVGs can be detrimental for their load alleviation performance, as discussed for $w/h = 2$. As a consequence, a larger number of SVGs is required to provide a sufficient lift reduction, leading to a considerable drag increase. In addition, it should be considered that the main cause of this limited lift reduction is the generation of strong suction peaks between the vortex vanes, which results in very high local speeds and additional normal shocks. Besides the loss of aerodynamic efficiency, this phenomenon can lead to structural implications such as excessive vibrations and fatigue issues. However, if a significant lift reduction is required ($\Delta C_L > 0.3$), low-aspect ratio SVGs were found to provide the best performance thanks to their mutual interaction, with minimum drag generation and a more uniform flow separation downstream of the SVG line; therefore, their use is recommended for load alleviation purposes.

It is worthwhile underlining that the vortex vane height was fixed in the analysis presented in this section. Based on the patterns observed in Sect.III, it is reasonable to expect that larger heights would lead to similar behaviours to those observed for $w/h \leq 4$ even at smaller aspect ratios, since high SVGs can already induce a full flow separation at small w/h. Conversely, shorter SVGs are expected to exhibit similar behaviour to those observed for low aspect ratio in the current study. Nonetheless, further analyses would be needed to determine the optimal vane height value, along with the aspect and wall ratios, for specific applications.

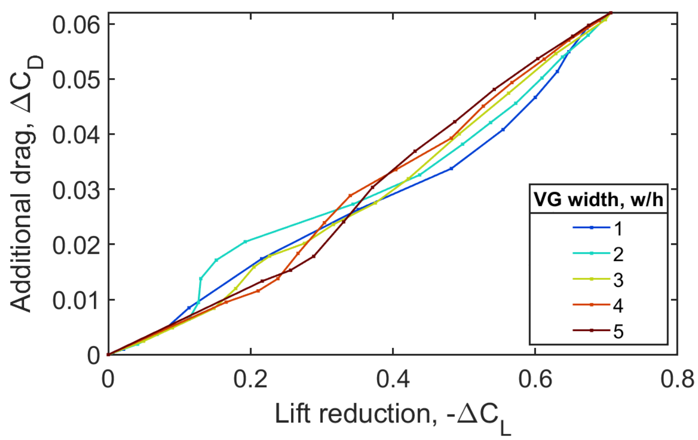

Fig. 21 Lift coefficient reduction vs additional generated drag coefficient in nominal cruise conditions (α = 2.15 deg) for $h/c = 0.02$ and varying aspect ratio.

VI. Conclusion

This paper presented a comprehensive analysis of the aerodynamic performance of switchable vortex generators (SVGs) operated in their spoiler configuration to perform load alleviation at transonic speeds. Three-dimensional computational fluid dynamics simulations were performed to investigate the effect produced by these devices on the aerodynamic forces acting on a simplified wing geometry, obtained as a straight extrusion of a supercritical airfoil, when varying geometric parameters such as the height and aspect ratio of the vortex vane, as well as changing the number of SVGs and their distance.

This study demonstrated that finite-span spoiler devices, such as the spoiler configuration of the SVG, can be effectively used to perform aerodynamic load alleviation. In particular, it was found that distinct aerodynamic regimes can be obtained by varying the SVG's vane height and aspect ratio. These regimes are characterised by absent, limited, or full flow separation downstream of the SVG, which significantly impacts load alleviation performance. Notably, sudden reductions in the lift coefficient can occur in the transition from partial to full flow separation regimes. Such different aerodynamic behaviours can also be observed in high-speed off-design conditions characterised by varying angle of attack. In this case, full separation downstream of the SVGs is observed to occur at small or negative incidence for larger devices, and at larger angles of attack if smaller vortex vanes are considered. In this latter case, transonic phenomena can also lead to sudden variation of the lift coefficient, resulting in undesirable aerodynamic behaviour.

When multiple finite-span SVGs are placed on the wing upper surface, their load alleviation performance is strongly affected by their mutual interaction, leading to different aerodynamic behaviour from that induced by a single SVG. The interaction among multiple SVGs was shown to be influenced by parameter such as their spacing and aspect ratios, emphasizing the critical role of the wall ratio parameter, i.e., the fraction of wingspan occupied by the vortex vanes in spoiler configuration, in establishing the aerodynamic performance. Smaller SVGs were observed to provide limited performance in lift reduction at low wall ratios, where their interaction can generate strong negative pressure peaks and supersonic regions between the vortex vanes, reducing the flow separation downstream of each device. However, low-aspect ratio SVGs become highly effective at high wall ratios, where they form an almost continuous wall with full separation extending across the entire wing upper surface downstream of the SVGs line. Conversely, larger SVGs proved more effective at low wall ratios, where they can generate full flow separation downstream of each device independently of their interaction, but showed a less effective lift reduction at higher wall ratios, due to the larger gaps still remaining among the vortex vanes. Remarkably, asymmetry and aperiodicity were observed in the flow distributions generated by multiple SVGs at high wall ratios, suggesting that the intrinsic nonlinearity of the problem may lead to multiple possible solutions. Nonetheless, results also indicated that lift alleviation performance is not strongly affected by such behaviours, and can still be predicted by referring to the curves obtained by studying the interaction of two SVGs only at given wall ratio.

Overall, the results presented in this paper highlight the potential of SVGs to provide robust load alleviation across a wide range of flight conditions, enabling a balance between structural weight reduction and aerodynamic performance. The findings from the parametric analysis can provide useful guidelines for design of finite-span spoiler devices for load alleviation. For instance, in applications where a significant lift reduction must be achieved on a given wingspan, low-aspect ratio devices should be preferred, since they can provide the required load alleviation at lower wall ratios, also reducing the associated drag generation. Nonetheless, in the SVG application, the parameter selection must also account for the requirements for the vortex generator functionality in high-lift settings, which remain under investigation. Regarding the spoiler function, further research is needed to refine the implementation of SVGs in more complex 3D wing geometries, including effects of wing sweep and taper. Additionally, experimental validation of the CFD findings is essential to confirm the performance of SVGs, particularly in those configuration where asymmetric flow distributions introduce a degree of uncertainty in the numerical results.

Acknowledgements

The work presented herein has been partially funded by the European Community's Clean Aviation programme under the Grant Agreement 101101974. The UPWing project (Ultra-Performance Wing) is a project funded under the topic Climate, Energy and Mobility, involving 26 partners. The project started on January 1, 2023.

Disclaimer

Co-Funded by the European Union. Views and opinions expressed are however those of the authors only and do not necessarily reflect those of the European Union or Clean Aviation Joint Undertaking. Neither the European Union nor the granting authority can be held responsible for them.

CLEAN AVIATION

Co-funded by
the European Union

References

[1] Eberle, A., Stefes, B., and Reckzeh, D., "Clean Aviation Ultra-Performance Wing (UP-Wing)," *AIAA Scitech 2024 Forum*, AIAA 2024-2109, 2024. https://doi.org/10.2514/6.2024-2109.

[2] Regan, C., and Jutte, C., "Survey of Applications of Active Control Technology for Gust Alleviation and New Challenges for Lighter-weight Aircraft," *Tech. Rep. NASA/TM-2012-216008*, 2012.

[3] Marino, L., Kiat, I., Eberle, A., and Sodja, J., "Parametric study of a switchable vortex generator for load alleviation in transonic conditions," *AIAA Scitech 2024 Forum*, AIAA 2024-2110, 2024. https://doi.org/10.2514/6.2024-2110.

[4] Taylor, H. D., "The elimination of diffuser separation by vortex generators," *United Aircraft Corporation Report No. R-4012-3*, 1947.

[5] Lin, J. C., "Review of research on low-profile vortex generators to control boundary-layer separation," *Progress in Aerospace Sciences*, Vol. 38, No. 4-5, 2002, pp. 389–420. https://doi.org/10.1016/S0376-0421(02)00010-6.

[6] Ashill, P., Fulker, J., and Hackett, K., "Research at DERA on sub boundary layer vortex generators (SBVGs)," *AIAA 2001–0887*, 2001. https://doi.org/10.2514/6.2001-887.

[7] Ashill, P., Fulker, J., and Hackett, K., "Studies of flows induced by sub boundary layer vortex generators," *AIAA 2002-0968*, 2002. https://doi.org/10.2514/6.2002-968.

[8] Ashill, P., Fulker, J., and Hackett, K., "A review of recent developments in flow control," *The Aeronautic Journal*, Vol. 109, No. 1095, 2005, pp. 205–232. https://doi.org/10.1017/S0001924000005200.

[9] Sørensen, N. N., Zahle, F., Bak, C., and Vronsky, T., "Prediction of the Effect of Vortex Generators on Airfoil Performance," *Journal of Physics: Conference Series*, Vol. 524, 2014, p. 012019. https://doi.org/10.1088/1742-6596/524/1/012019.

[10] Lin, J. C., "Control of turbulent boundary-layer separation using micro-vortex generators," *30th Fluid Dynamics Conference*, AIAA 99-3404, 1999. https://doi.org/10.2514/6.1999-3404.

[11] Wendt, B., "Parametric study of vortices shed from airfoil vortex generators," *AIAA Journal*, Vol. 42, No. 11, 2004, pp. 2185–2195. https://doi.org/10.2514/1.3672.

[12] Tebbiche, H., and Boutoudj, M. S., "Vortex Generators Contribution to the Enhancement of the Aerodynamic Performances," *Advanced Materials Research*, Vol. 950, 2014, pp. 268–274. https://doi.org/10.4028/www.scientific.net/AMR.950.268.

[13] Gao, L., Zhang, H., Liu, Y., and Han, S., "Effects of vortex generators on a blunt trailing-edge airfoil for wind turbines," *Renewable Energy*, Vol. 76, No. 5, 2015, pp. 303–311. https://doi.org/10.1016/j.renene.2014.11.043.

[14] Fouatih, O., Medale, M., Imine, O., and Imine, B., "Design optimization of the aerodynamic passive flow control on NACA 4415 airfoil using vortex generators," *European Journal of Mechanics - B/Fluids*, Vol. 56, 2016, pp. 82–96. https://doi.org/10.1016/j.euromechflu.2015.11.006.

[15] Baldacchino, D., Ferreira, C., De Tavernier, D., Timmer, W., and van Bussel, G., "Experimental parameter study for passive vortex generators on a 30% thick airfoil," *Wind Energy*, Vol. 21, No. 9, 2018, pp. 745–765. https://doi.org/10.1002/we.2191.

[16] Li, X.-K., Liu, W., Zhang, T.-J., Wang, P.-M., and X-D, W., "Analysis of the Effect of Vortex Generator Spacing on Boundary Layer Flow Separation Control," *Applied Sciences*, Vol. 9, No. 24, 2019, p. 5495. https://doi.org/10.3390/app9245495.

[17] Li, X.-K., Liu, W., Zhang, T.-J., Wang, P.-M., and X-D, W., "Experimental and Numerical Analysis of the Effect of Vortex Generator Installation Angle on Flow Separation Control," *Energies*, Vol. 12, No. 23, 2019, p. 4583. https://doi.org/10.3390/en12234583.

[18] Liebeck, R. H., "Design of Subsonic Airfoils for High Lift," *Journal of Aircraft*, Vol. 15, No. 9, 1978, pp. 547–561. https://doi.org/10.2514/3.58406.

[19] Li, Y., Wang, J., and Zhang, P., "Influences of Mounting Angles and Locations on the Effects of Gurney Flaps," *Journal of Aircraft*, Vol. 40, No. 3, 2003, pp. 494–498. https://doi.org/10.2514/2.3144.

[20] Wang, J., Li, Y., and Choi, K.-S., "Gurney flap—Lift enhancement, mechanisms and applications," *Progress in Aerospace Sciences*, Vol. 44, No. 1, 2008, pp. 22–47. https://doi.org/10.1016/j.paerosci.2007.10.001.

[21] Li, Y., Wang, J., and Hua, J., "Experimental investigations on the effects of divergent trailing edge and Gurney flaps on a supercritical airfoil," *Aerospace Science and Technology*, Vol. 11, No. 2–3, 2007, pp. 91—-99. https://doi.org/10.1016/j.ast.2006.01.006.

[22] Yen Nakafuji, C., D.T. van Dam, Smith, R., and Collins, S., "Active Load Control for Airfoils Using Microtabs," *Journal of Solar Energy Engineering*, Vol. 123, No. 4, 2001, pp. 282—-289. https://doi.org/10.1115/1.1410110.

[23] Mayda, E., van Dam, C., and Yen-Nakafuji, D., "Computational Investigation of Finite-Width Microtabs for Aerodynamic Load Control," *43rd AIAA Aerospace Sciences Meeting and Exhibit*, AIAA 2005-1185, 2005. https://doi.org/10.2514/6.2005-1185.

[24] Chow, R., and van Dam, C. P., "Unsteady Computational Investigations of Deploying Load Control Microtabs," *Journal of Aircraft*, Vol. 43, No. 5, 2006, pp. 1458–1469. https://doi.org/10.2514/1.22562.

[25] Cooperman, A. M., Chow, R., and van Dam, C. P., "Active Load Control of a Wind Turbine Airfoil Using Microtabs," *Journal of Aircraft*, Vol. 50, No. 4, 2013, pp. 1150–1158. https://doi.org/10.2514/1.C032083.

[26] Baker, J., Standish, K., and van Dam, C., "Two-Dimensional Wind Tunnel and Computational Investigation of a Microtab Modified Airfoil," *Journal of Aircraft*, Vol. 44, No. 2, 2007, pp. 563—-572. https://doi.org/10.2514/1.24502.

[27] Jacobs, E., "Airfoil Section Characteristics as Affected by Protuberances," Tech. rep., NACA TR 446, 1934.

[28] Heathcote, D. J., Gursul, I., and Cleaver, D. J., "An Experimental Study of Minitabs for Aerodynamic Load Control," *54th AIAA Aerospace Sciences Meeting*, AIAA Paper 2016-0325, 2016. https://doi.org/10.2514/6.2016-0325.

[29] Heathcote, D. J., Gursul, I., and Cleaver, D. J., "Aerodynamic Load Alleviation Using Minitabs," *Journal of Aircraft*, Vol. 55, No. 5, 2018, pp. 2068–2077. https://doi.org/10.2514/1.C034574.

[30] Bull, S., Chiereghin, N., Cleaver, D., and Gursul, I., "Novel approach to leading-edge vortex suppression," *AIAA Journal*, Vol. 58, No. 10, 2020, pp. 4212—4227. https://doi.org/10.2514/1.J059444.

[31] Hadjipantelis, M., Son, O., Wang, Z., and Gursul, I., "Frequency response of separated flows on a plunging finite wing with spoilers," *Experiments in Fluids*, Vol. 65, No. 36, 2024, pp. 1—27. https://doi.org/10.1007/s00348-024-03775-3.

[32] Lock, R. C., "An equivalence law relating three-and two-dimensional pressure distributions," *Aeronautical Research Council Reports and Memoranda*, Vol. 3346, 1962.

[33] Wild, J., *High-Lift Aerodynamics*, 1st ed., CRC Press, Boca Raton, FL, 2022.

[34] Xu, Z.-M., Han, Z.-H., and Son, W.-P., "An improved 2.75D method relating pressure distributions of 2D airfoils and 3D wings," *Aerospace Science and Technology*, Vol. 128, 2022, p. 107789. https://doi.org/10.1016/j.ast.2022.107789.

[35] Menter, F. R., "Zonal Two Equation k/omega, Turbulence Models for Aerodynamic Flows," *AIAA Journal*, Vol. 32, No. 8, 1993, pp. 1993–2006. https://doi.org/10.2514/6.1993-2906.

[36] Menter, F. R., "Two-Equation Eddy-Viscosity Turbulence Models for Engineering Applications," *AIAA Journal*, Vol. 32, No. 8, 1994, pp. 1598–1605. https://doi.org/10.2514/3.12149.

[37] Anderson, J. D., *Fundamentals of Aerodynamics*, 4th ed., McGraw Hill, New York, 2007.